



Anisotropic fracture forming limit curve and its applications for sheet metal forming with complex strain paths of aluminum sheet

Taratip Chaimongkon¹ · Sansot Panich¹ · Vitoon Uthaisanguk² 

Received: 13 January 2021 / Accepted: 26 May 2021 / Published online: 8 June 2021
© The Author(s), under exclusive licence to Springer-Verlag London Ltd., part of Springer Nature 2021

Abstract

In this work, formabilities of aluminum sheet alloy grade AA5052-H32 were investigated under consideration of the anisotropic behavior of material. Experimental tensile tests and modified Marciniak in-plane stretch-forming tests of sheet samples with varying shapes were performed for different sample orientations. The critical fracture strains at various states of stress were gathered by means of a digital image correlation (DIC) technique. Then, the Lou-Huh ductile fracture criterion was applied in combination with the Hill'48 and Yld2000-2d yield criteria for generating the fracture loci (FLs) of examined sheet. Hereby, material parameters of the fracture model were calibrated by the tensile tests of pure shear, uniaxial tension and plane strain samples. It was found that the Yld2000-2d-based fracture model could more accurately predict the experimental limit strains at all stress states. In addition, the representative anisotropic FL was proposed and transformed to fracture forming limit curve (FFLC), which was afterwards verified by a cross die forming test and a square cup drawing test. The predicted force-displacement curves, moment of fracture onsets, and fracture sites of samples positioned in different directions were well in accordance with the experimental results. The state of stress and material anisotropy strongly affected the fracture occurrences of tested samples. The representative FFLC by the Lou-Huh model and the Yld2000-2d yield function more accurately described the forming limits of investigated aluminum sheet.

Keywords Anisotropic fracture forming limit curve; · Aluminum sheet alloy; · Marciniak stretch-forming test; · Cross die forming test · Square cup drawing test

1 Introduction

In the age of technological disruption, extraordinarily creative product designs are definitely inevitable to satisfy rapidly fluctuating customer needs. Such multiple changes are certainly applied to the sheet metal forming industry as well for the sake of survival. Hereby, sophisticated forming procedures and

conditions were entailed by manufacturing contemporary forming work pieces. The sheet metal forming has been widely applied in the industries for part making of vehicles due to their extremely diverse geometries. For automobile bodies, low carbon steel sheets have been mostly used in the past. Recently, lightweight car body components have become one of the highest priorities in the development of the automotive industry, in which it is strictly required to satisfy environment friendly car by consuming less energy. Therefore, aluminum alloys have been increasingly applied in the commercial automobiles as well as in other applications such as racing cars and aircrafts, as shown in Sekhar et al. [1]. For this purpose, there has been a need to understand the evolution of strain localization and fracture mechanism of aluminum sheets during forming processes. Effects of strain path changes and plastic anisotropy on their formabilities must be taken into account in order to obtain forming parts with desired shape and no defect.

During the last half-century, many evaluation methods have been proposed for assessing the formability of sheet

✉ Sansot Panich
sansot.p@eng.kmutnb.ac.th

✉ Vitoon Uthaisanguk
vitoon.uth@kmutt.ac.th

¹ Department of Production Engineering, Faculty of Engineering, King Mongkut's University of Technology North Bangkok, 1518 Pracharat 1 Road, Wongsawang, Bangsue, Bangkok 10800, Thailand

² Centre for Lightweight Materials, Design and Manufacturing, Department of Mechanical Engineering, Faculty of Engineering, King Mongkut's University of Technology Thonburi, 126 Pracha Uthit Road, Bang Mod, Thung Khru, Bangkok 10140, Thailand

materials. One of the most popular tools is a forming limit diagram (FLD), which was first proposed by Keeler and Backofen [2] and Goodwin [3] and has been widely employed to evaluate localized necking and thickness reduction of sheet metals until today. Nevertheless, conventional FLD is not appropriate for prediction of fracture in aluminum, magnesium alloys as well as advanced high strength steels (AHSSs), since these metals fail with a little amount of necking that was differed from other conventional sheet alloys. Thus, a precise description of fracture onset of such materials by the FLD is limited and very challenging. Otherwise, ductile fracture criteria have been another capable predictive tool for occurred failures of these sheet metals, which were commonly observed in a shear stress region or where stress triaxiality value was low, as reported by Bao and Wierzbicki [4], Børvik et al. [5] and Khan and Liu [6, 7]. Hence, a sudden fracture of aluminum sheets in metal forming could be well described by the ductile fracture criterion. Generally, formation of macroscopic cracks in metal sheets was often considered as the result of damage accumulation in material at a mesoscopic and/or microscopic level [8]. In the context of ductile fracture, damage was basically provided as a consequence of void evolution [9, 10]. Chu and Needleman [11] and LeRoy et al. [12] improved the concept by taking into consideration void coalescence and void nucleation at elevated strain. In addition, different analytical, numerical studies and experimental works were carried out for example in Cockcroft and Latham [13], Brozzo et al. [14], Oh et al. [15], Oyane et al. [16], Clift et al. [17], and Ko et al. [18] in order to predict ductile fracture of metals in various forming processes. In the last decade, such ductile fracture models have been successfully utilized in bulk forming processes like upsetting, axisymmetric extrusion, strip compression and tension due to their few parameters and simple calibration with experimental data. However, many failure criteria are incapable of fully describing ductile fracture behavior over a wide range of stress states, especially observed in complex sheet forming procedures.

Bao and Wierzbicki [4] determined fracture strains of aluminum sheet samples grade AA 2024-T351 from compression, shear up to tension deformation region. From their experiments, a fracture locus (FL) of the examined sheets was presented in wide range of stress triaxiality. Afterwards, several ductile fracture models were introduced similar to this work. A modified Mohr-Coulomb (MMC) fracture model of aluminum AA6061-T6 sheet was presented by Bai and Wierzbicki [19], which showed a good balance between the complexity of physical basis and the simplicity needed for practical industrial applications. Another ductile fracture model was proposed by Lou et al. [20], in which the nucleation of voids was a function of equivalent plastic strain, growth of voids was described by the stress triaxiality and coalescence of voids was controlled by the normalized maximum shear stress resulting in shear cross linking. These three mechanisms

should be properly incorporated when describing fracture of aluminum sheets. Furthermore, rolled sheet metals exhibited anisotropy which not only affected their plastic deformation response but also the initiation of fracture. Banabic [21] provided a comprehensive modeling of anisotropic properties of metal sheets. The loading direction strongly influenced stress-strain and fracture behavior of material, as shown in [22]. Benzerga et al. [23, 24] studied effects of specimen orientation on anisotropic deformation and fracture of a low alloy medium strength steel. A theory of anisotropic ductile fracture was introduced, in which plastic anisotropy and microstructure evolution including porosity, void shape, orientation and spacing were considered. It was reported that void nucleation and crack propagation exhibited anisotropic characteristics and a physically based void coalescence model should be thus used. Beese et al. [25] developed a partially coupled anisotropic fracture model by coupling the Hill'48 yield function with the MMC criterion for aluminum grade 6061-T6. Luo et al. [26] extended the isotropic MMC model to a non-associated anisotropic fracture model for AA 6260-T6, in which a stress state dependent weighting function and transformed anisotropic plastic strains were applied. Lou and Yoon [27] showed that the anisotropic model could accurately illustrate the directionality in ductile fracture of AA 6K21-IH T4. Park et al. [28] modified the isotropic Lou-Huh ductile fracture criterion to take into account the anisotropy effects of material on the equivalent plastic strain at fracture onset by using Hill'48 model. Park et al. [29] introduced an anisotropic FFLC of AHSS sheets with regard to the isotropic biaxial fracture strain. Lou and Yoon [30] developed a ductile fracture criterion by coupling the Drucker function with the first stress invariant. Hereby, the Drucker model was modified to incorporate the effects of stress triaxiality and normalized third invariant on ductile fracture of aluminum grade AA2024-T351. Li et al. [31] designed a double-notched shear specimen in order to precisely measure the out-of-plane shear fracture strength of steel sheet grade 980. An anisotropic ductile fracture model based on linear transformation of stresses was hereby presented to consider shear fracture mechanism of investigated steel.

In Young [32], the MMC fracture loci were transformed into the space of principal strains by a plane stress plasticity theory and compared with experimental results for various materials. Bai [33] constructed FFLC from MMC fracture envelope under consideration of proportional loading and associated flow rule. Li et al. [34] showed that the MMC fracture locus of an AHSS grade that consisted of four regions in the space of equivalent strain to fracture and stress triaxiality. They further transformed the FL into FFLC with two new branches, which represented the formation of shear-induced fracture. Chen et al. [35] reported that the equivalent plastic strain based FLC (ep-FLC) well described the results of a two-step nonlinear test. Then, the feasibility of complex three-

stage stamping process for a wheel disc was performed by FE simulations using both traditional FLC and ep-FLC. It was found that the critical location and forming state of fracture onset could be more precisely predicted by the ep-FLC. Manopulo et al. [36] proposed a systematic approach for evaluating the effects of anisotropic hardening models with the least possible disturbance from real experimental conditions such as blank holder force, friction and tool deflection. The hardening models were combined with the Yld2000-2d yield criterion and applied for investigating a mild steel grade DC05 in two deep drawing processes, in which measured and calculated strain distributions were compared. Gorji et al. [37] introduced a strain localization level based model for predicting the necking phenomenon. The so-called thinning method was used to obtain the critical fracture strains, in which the thickness of corresponding fracture site was measured. 3-point bending tests of various pre-strained specimens were performed to validate the presented fracture model. It was hereby reported that the triaxiality at failure point was independent on the deformation path. Pack et al. [38] determined the parameters of Hosford-Coulomb fracture criterion for DP980 steel grade from the uniaxial tension, simple shear and V-bending and punch experiments and validated the model predictions through the Nakajima, tension and bending of specimens with different notch radii. It was shown that the domain of shell-to-solid equivalence was required when using shell elements in order to ensure the convergence of ductile fracture initiation. The fracture model acceptably predicted the onset of ductile failure for both membrane- and bending-dominated loading conditions. Talebi-Ghadikolaee et al. [39] calibrated the material parameters of the modified Mohr-Coulomb (MMC) fracture criterion by means of a uniaxial, plane strain, notched, and modified in-plane shear tension tests. The calibrated model could represent the fracture occurrence in a U-bending process of the AA6061-T6 aluminum alloy sheet with acceptable accuracy. It was also shown that the effects of process parameters on the stress state could be negligible. Panich et al. [40] determined the damage loci for predicting both ductile damage initiation and fracture of the AHSS grade JAC780Y. The damage loci were then transformed to FFLCs, which could fairly describe formabilities of the examined steel. Moreover, Charoensuk et al. [41] constructed damage initiation loci, FLs and respective FFLCs for two AHSS grades taking into account effects of material anisotropy.

It is seen that ductile fracture formation of thin sheet metals has not been well understood because of the coexistence of complex fracture mechanism including void evolution and shear fracture. On the other hand, a universal, relatively simple model and corresponding standard calibration procedure are required for the industry. A more precise prediction and experimental investigations of anisotropic ductile fracture of sheet metals is still challenging. In this work, it was thus aimed to study the anisotropic fracture behavior of AA5052-H32

aluminum sheet. First, Marciniak in-plane stretching tests and tensile tests of various notched samples were conducted. Three different loading directions regarding the rolling direction of sheet were examined. Subsequently, the Lou-Huh ductile fracture criterion in combination with the anisotropic Hill'48 and Yld2000-2d yield functions were applied to generate FLs of the investigated sheet. The Lou-Huh model has been coupled with other anisotropic yield functions except the Barlat2000 model. A methodology for transforming experimental fracture strain data to stress triaxiality and plastic strain locus, in which the anisotropic Yld2000-2d model was combined, was presented. Then, the material parameters were calibrated and the predicted results were validated with the experimentally obtained data. Moreover, the determined anisotropic FL were transformed into FFLC and then used for evaluating failure occurrences of aluminum sheets during a cross die forming and square cup drawing test. The prediction accuracies of the FFLCs were finally discussed.

2 Modelling of anisotropic fracture locus

In this work, threshold loci for fracture of aluminum grade AA5052-H32 were generated by using the Lou-Huh ductile fracture criterion. The employed construction of FL was coupled with two anisotropic yield criteria, namely, Hill'48 and Yld2000-2d model. The constitutive equations and step-wise procedures for predicting the FL are given as following.

2.1 Fracture loci

The Lou-Huh ductile fracture criterion [20] defines damage accumulation of sheet metal, in which the void evolution in ductile material is incorporated. The criterion is described in Eq. (1).

$$\left(\frac{2\tau_{\max}}{\bar{\sigma}}\right)^{C_1} \cdot \left(\frac{\langle 1+3\eta \rangle}{2}\right)^{C_2} \cdot \bar{\epsilon}_f = C_3 \langle x \rangle = \begin{cases} x & \text{when } x \geq 0 \\ 0 & \text{when } x < 0 \end{cases} \quad (1)$$

τ_{\max} is the maximal shear stress, $\bar{\sigma}$ is the equivalent stress, η is the stress triaxiality, $\bar{\epsilon}_f$ is the equivalent plastic strain to fracture and C_1 , C_2 , C_3 are material constants. This model takes into account all three main damage accumulating mechanisms, namely, nucleation, growth and shear coalescence of voids. Hereby, the void nucleation was assumed to be proportional to the equivalent plastic strain under uniaxial tension $\bar{\epsilon}_f$. During plastic deformation, the void growth was represented in a relationship with the stress triaxiality $(1+3\eta)$, whereas the shear coalescence of voids was governed by the normalized maximal shear stress to effective stress $(\tau_{\max}/\bar{\sigma})$. Two exponents C_1 and C_2 were introduced to the first and second term

in order to modulate the different impacts of void nucleation, growth and coalescence on a resulting ductile fracture. The material constant C_1 was the ratio of equivalent plastic strain to fracture in the uniaxial tension to those in the pure shear and plane strain. When C_1 became large, the influence of shear stress on the ductile fracture increased and the rupture strain was therefore reduced. Basically, high mean stress led to an acceleration of void growth, whereas the growth of voids was suppressed by a negative mean stress and fracture was then delayed. Hence, the equivalent plastic strain to fracture became lower at higher stress triaxiality range though the normalized maximal shear stress was equal in both plane strain and pure shear states. The material constant C_3 was related to the equivalent plastic strain to fracture of the uniaxial tension state $\bar{\varepsilon}_t$, which could be obtained by a hybrid experimental-numerical method using DIC technique, as shown in Bao and Wierzbicki [4] and Dunand and Mohr [42]. The constant C_3 varied the magnitude of FL without an influence on its shape.

For the determination of these three materials parameters of the Lou-Huh model, at least three experimental tests, namely, uniaxial tensile test, plane strain test, pure shear test and hydraulic bulge test or balanced biaxial tensile test were required. At each state of stress, the ductile fracture criterion was reduced to a simple equation. For a uniaxial tension ($\tau_{\max}/\bar{\sigma} = 1/2$ and $\eta = 1/3$), the material constant C_3 could be derived as followed.

$$C_3 = \bar{\varepsilon}_t \quad (2)$$

Under a plane strain condition ($\tau_{\max}/\bar{\sigma} = \eta = 1/\sqrt{3}$), Eq. (1) was expressed in the form as given in Eq. (3), by which $\bar{\varepsilon}_p$ was the equivalent plastic strain to fracture at the plane strain state.

$$\left(\frac{2}{\sqrt{3}}\right)^{C_1} \cdot \left(\frac{1+\sqrt{3}}{2}\right)^{C_2} \cdot \bar{\varepsilon}_p = C_3 \quad (3)$$

In the case of balanced biaxial tension ($\tau_{\max}/\bar{\sigma} = 1/2$ and $\eta = 2/3$), Eq. (1) became Eq. (4), in which $\bar{\varepsilon}_b$ was the equivalent plastic strain to fracture at the biaxial tension state.

$$\left(\frac{3}{2}\right)^{C_2} \cdot \bar{\varepsilon}_b = C_3 \quad (4)$$

At a pure shear condition ($\tau_{\max}/\bar{\sigma} = 1/\sqrt{3}$ and $\eta = 0$), Eq. (1) was reduced to Eq. (5) with $\bar{\varepsilon}_s$ as the equivalent plastic strain to fracture at the pure shear state.

$$\left(\frac{2}{\sqrt{3}}\right)^{C_1} \cdot \left(\frac{1}{2}\right)^{C_2} \cdot \bar{\varepsilon}_s = C_3 \quad (5)$$

All these states of stress could not be fully achieved in a practical experiment due to necking and other imperfection factors. More experimental data points were certainly preferred for constructing a more precise FL of sheet metal by

the model. It is noted that the values of all three material constants must be positive in order to obtain the acceptable magnitudes of predicted fracture strains in each stress region. Using the Lou-Huh ductile fracture criterion and experimentally gathered material parameters, FL of the investigated aluminum could be hereby predicted.

2.2 Coupling of the anisotropic behavior

In order to incorporate plastic anisotropic characteristics of the aluminum sheet by the determination of its ductile fracture limit or FL the Hill' 48 and Yld2000-2d yield functions were applied. For the calculations, the strain ratio (ρ) and stress ratio (α), which were previously proposed by Butuc et al. [43] for an isotropic condition, as given in Eq. (6) and Eq. (7), respectively, were considered.

$$\rho = \frac{\varepsilon_2}{\varepsilon_1} \quad (6)$$

$$\alpha = \frac{\sigma_2}{\sigma_1} \quad (7)$$

$\varepsilon_1, \varepsilon_2$ are two principal in-plane strains ($\varepsilon_1 \geq \varepsilon_2$) and σ_1, σ_2 are two principal in-plane stresses ($\sigma_1 \geq \sigma_2$). The general relationship between the strain and stress ratios are provided as followed.

$$\alpha = \frac{2\rho + 1}{2 + \rho} \quad (8)$$

For the in-plane condition of an isotropic material and by the absence of shear stress in a coordinate system that aligned with the anisotropy axes, the major true stress could be defined by the relationship between the equivalent stress ($\bar{\sigma}$) and the stress ratio parameter (ξ), as expressed in Eq. (9).

$$\sigma_1 = \frac{\bar{\sigma}}{\xi} \quad (9)$$

Then, the equivalent plastic strain ($\bar{\varepsilon}$) could be derived in dependence on the maximum principal strains (ε_1) by means of Eq. (10).

$$\bar{\varepsilon} = \varepsilon_1 \cdot (1 + \rho \cdot \alpha) / \xi \quad (10)$$

2.2.1 Hill'48 model

The anisotropic Hill'48 yield criterion was described by a quadratic function according to the principal axes, which usually coincided with the rolling, transverse and normal directions of the sheet sample, as shown in Eq. (11).

$$\varphi(\sigma) = \bar{\sigma}_{\text{Hill}}^2 = F\sigma_{yy}^2 + G\sigma_{xx}^2 + H(\sigma_{xx} - \sigma_{yy})^2 + 2N\sigma_{xy}^2 \quad (11)$$

where $F, G, H,$ and N were the parameters, which represented the current state of anisotropic yielding behavior of material, σ_{xx}, σ_{yy} were the principal stresses ($\sigma_{xx} = \sigma_1$ and $\sigma_{yy} = \sigma_2$) and σ_{xy} was the shear stress component. As reported in Stoughton [44], the material parameters of the Hill'48 function could be treated as dependencies regarding the tensile and shear yield stresses associated to the principal anisotropic directions. Therefore, the relationship between the strain ratio and stress ratio and the stress ratio parameter with consideration of anisotropic characteristic were derived with regard to the Hill'48 yield function, as provided in Eq. (12) and Eq. (13), respectively.

$$\rho_{Hill} = \frac{(F + H) \cdot \alpha - H}{G + H - H\alpha} \tag{12}$$

$$\xi_{Hill} = \frac{\bar{\sigma}_{Hill}}{\sigma_1} = \sqrt{(G + H) + (F + H)\alpha^2 - 2H\alpha} \tag{13}$$

In this work, the Hill'48 material parameters were gathered by using the r -value based approach. The r -values along three loading directions, namely, r_0 (parallel direction, RD), r_{45} (diagonal direction, DD) and r_{90} (transverse direction, TD) to the rolling direction of sheet metal were firstly determined by experimental tensile tests in varying directions. The relationships between the r -values and Hill's parameters $F, G, H,$ and N were derived by the associative flow rule, as given in Eq. (14).

$$H = \frac{r_0}{1 + r_0}, G = \frac{1}{1 + r_0}, \frac{F}{H} = \frac{1}{r_0} \text{ and } N = \frac{(r_0 + r_{90}) \cdot (1 + 2r_{45})}{2r_{90} \cdot (1 + r_0)} \tag{14}$$

2.2.2 Yld2000-2d model

The Yld2000-2d yield criterion generally represented a non-quadratic yield behavior of sheet metal, as proposed by Barlat et al. [45]. The expression of this model is provided in a form of the deviatoric stresses, as shown in Eq. (15).

$$\phi(\sigma) = 2\bar{\sigma}_B^a = \left| \tilde{S}'_1 - \tilde{S}'_2 \right|^a + \left| 2\tilde{S}''_2 + \tilde{S}''_1 \right|^a + \left| 2\tilde{S}''_1 + \tilde{S}''_2 \right|^a \tag{15}$$

where \tilde{S}'_i and \tilde{S}''_i ($i = 1, 2$) denoted the principal values of the stress tensors, which were described by the stress vectors \tilde{S} and \tilde{S}'' ($\tilde{S} = L' : \sigma$ and $\tilde{S}'' = L'' : \sigma$), respectively. The exponent a was the material constant. Hereby, the linear transformations L' and L'' were specified through the eight material parameters (α_1 to α_8). These eight anisotropic parameters of the Yld2000-2d model could be derived in conjunction with a system of non-linear algebraic formulations, as reported in Barlat et al. [45] and Yoon et al. [46]. Otherwise, the yield stresses, $\sigma_0, \sigma_{45}, \sigma_{90}, \sigma_b$ and r -values, r_0, r_{45}, r_{90}, r_b were required

for the calculations, in which a series of experimental tests including uniaxial tensile tests of different sheet orientations, biaxial test, disk compression test was carried out. Subsequently, in the principal plane, the strain ratio could be rewritten as a function of the stress ratio with consideration of the plastic anisotropy of material with respect to the Yld2000-2d yield model, as shown in Eq. (16). More details could be found in Basak and Panda [47].

$$\rho_{Yld} = \frac{-B'|A'-B'\alpha|^{(\alpha-1)} + D'|C'+D'\alpha|^{(\alpha-1)} + F'|E'+F'\alpha|^{(\alpha-1)}}{A'|A'-B'\alpha|^{(\alpha-1)} + C'|C'+D'\alpha|^{(\alpha-1)} + E'|E'+F'\alpha|^{(\alpha-1)}} \tag{16}$$

where, $A' = \frac{2\alpha_1 + \alpha_2}{3}, B' = \frac{2\alpha_2 + \alpha_1}{3}, C' = \frac{2\alpha_3 + \alpha_4}{3}, D' = \frac{4\alpha_4 + \alpha_3}{3}, E' = \frac{4\alpha_5 + \alpha_6}{3}, F' = \frac{2\alpha_6 + \alpha_5}{3}$. Moreover, the stress ratio parameter could be also presented in term of the stress ratio based on the Yld2000-2d yield function, as expressed in Eq. (17) [47].

$$\xi_{Yld} = \frac{\bar{\sigma}_{Yld}}{\sigma_1} = \left[\frac{1}{2} \left\{ |A'-B'\alpha|^a + |C'+D'\alpha|^a + |E'+F'\alpha|^a \right\} \right]^{1/a} \tag{17}$$

By means of Eq. (6), (8), (12), (13) and (16), (17), the strain ratios, stress ratios and stress ratio parameters could be determined for different sheet orientations and strain paths, in which the plastic anisotropy of material was considered with regard to the Hill' 48 and Yld2000-2d yield models, respectively. The equivalent plastic strains to fracture at each stress state were calculated for the experimentally gathered critical strains by using Eq. (10) and afterwards the material parameters C_1, C_2 and C_3 were derived with respect to Eq. (2), (3), (4), and (5), accordingly. Finally, the anisotropic FLs of the examined aluminum sheet could be predicted for the entire range of state of stress on the basis of different yield functions by the Lou-Huh fracture criterion.

Besides, in this work, the plastic strains at fracture of aluminum sheets from the experiments were directly calculated into the stress triaxialities and equivalent plastic strains, in which the anisotropic Hill'48 and Yld2000-2d yield criteria were incorporated by the stress ratio parameter (ξ) similar to the works in [47, 48]. The stress triaxiality (η) as the ratio between the means stress or hydrostatic stress (σ_m) and the equivalent stress and the equivalent plastic strain ($\bar{\epsilon}$) could be transformed from the experimental fracture strain pairs by using Eqs. (18) and (10), accordingly. The required strain ratios, stress ratios and stress ratio parameters were also derived as done for the construction of FL by the Lou-Huh model. It is noted that these pairs of stress triaxialities and equivalent plastic strains at fracture served as the experimental data for verifying the predicted FLs.

$$\eta = \left(\frac{1 + \alpha}{3} \right) \cdot \left(\frac{1}{\xi} \right) \tag{18}$$

Table 1 Chemical composition (mass content in %) of the examined aluminum sheet

Material	Mg	Cr	Fe	Si	Mn	Zn	Cu	Al
AA5052-H32	2.7826	0.1922	0.3396	0.0807	0.0427	0.0126	0.0130	Balanced

3 Characterization of material yield and hardening behavior

The investigated material in this work was the aluminum sheet grade AA5052-H32, which contained Mg as its major alloying element and small amounts of other alloying elements. The chemical compositions of the examined sheet are given in Table 1. This AA5052-H32 sheet exhibited relative good mechanical properties, formability, corrosion resistance, especially to salt water, and high fatigue strength. Such aluminum grade has been widely used in the aircraft components such as control surfaces, landing gear doors, leading edges, trailing edges, fuselage components, flooring and helicopter rotor blades. In order to generate the FLs of investigated aluminum sheet plastic yield and hardening behavior of material were characterized by means of various experiments including uniaxial tensile, hydraulic bulge and disk compression tests. The results were further applied for calculating the anisotropic parameters of the Hill'48 and Yld2000-2d models.

3.1 Uniaxial tensile test

Uniaxial tensile tests were carried out for obtaining stress-strain curves and material yield characteristics under different loading directions. The sheet specimens were prepared according to the ASTM-E8 standard along three sample orientations, namely, 0° (RD), 45° (DD) and 90° (TD) to the rolling direction. During the tests, a crosshead speed of machine was set to allow for the constant strain rate of 0.001 s⁻¹. As a result, the stress-strain curves of AA5052-H32 grade were gathered. Moreover, from the strains of two extensometers in the length and width of test specimens and the volume constancy, *r*-values were calculated. The yield strength (YS), ultimate tensile strength (UTS), uniform elongation and total elongation of tested sheet samples regarding RD, DD and TD are

Table 2 Determined tensile properties of the investigated aluminum sheet grade AA5052-H32

Test direction	YS (MPa)	UTS (MPa)	Elongation (%)	
			Uniform	Total
0°	191.91	250.89	10.24	14.2
45°	194.13	246.55	14.14	16.6
90°	201.53	256.04	11.91	13.5

summarized in Table 2. The determined plastic true stress-strain curves are demonstrated for all three loading directions in Fig. 1. At least three repeated tests were conducted and the results of each direction were close to each other. Obviously, the yield stress curves of AA5052-H32 specimens from all three orientations were somewhat deviated. The sheets showed the largest yield and tensile strengths, but lowest elongations at TD. The highest formability was obtained from the samples at DD. Nevertheless, the examined aluminum exhibited largely different *r*-values in each direction, as seen in Table 3. Furthermore, the normalized flow stresses and *r*-values are presented for varying orientations in Table 3.

3.2 Hydraulic bulge test

The three yield stresses σ_0 , σ_{45} , σ_{90} and three anisotropy parameters r_0 , r_{45} , r_{90} could be directly gathered from the experimental tensile tests. By calculating the anisotropic coefficients of Yld2000-2d yield criterion, material deformation under the balanced biaxial stress state needed to be additionally explored. To this purpose, a hydraulic bulge test was experimentally performed for obtaining the balanced biaxial yield stress (σ_b) of the investigated aluminum. Its schematic test setup is depicted in Fig. 2. More details of the test procedure and tool geometries can be referred to Alharthi et al. [49] and Panich et al. [40]. In the bulge test, stress-strain relationship was commonly described by the von Mises effective stress and strain, in which the balanced biaxial stress and thickness strain at the pole were considered as in Panich et al. [40] and Prakash [50]. According to the membrane theory, the balanced biaxial stress or membrane stress can be thus expressed as following.

$$\sigma_b = \frac{p}{2} \left(\frac{R_d}{t_d} + 1 \right) \quad (19)$$

where p and R_d are the hydrostatic pressure and radius of curvature, respectively. The thickness strain ε_b was derived with respect to the initial thickness t_0 and current thickness at the dome t_d of aluminum sheet. Note that the instantaneous dome

Table 3 Normalized flow stresses and *r*-values of the investigated aluminum sheet

AA5052-H32	0°	45°	90°	Balanced biaxial
Normalized flow stress	1.0000	1.0115	1.0501	1.1212
<i>r</i> -value	0.6545	0.9311	1.1513	0.9586

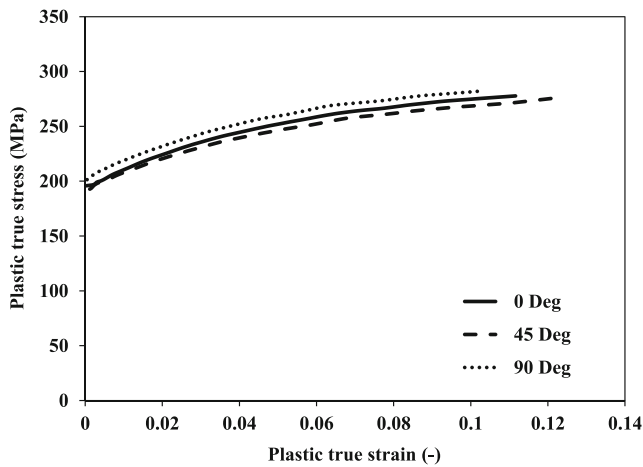


Fig. 1 Plastic true stress-true strain curves determined by uniaxial tensile tests of the investigated aluminum sheet grade AA5052-H32 in different loading directions

heights of formed sheet sample were measured by a LDVT and then applied for calculating the current sheet thickness and curvature radius, as reported in details in Nasser et al. [51].

$$\varepsilon_b = \ln\left(\frac{t_d}{t_0}\right) \tag{20}$$

From the measured pressures, curvature radii and thicknesses along with Eqs. (19) and (20), flow stress curve of the sheet was determined. Subsequently, the flow curve from the bulge test was fitted with the Swift hardening law, as illustrated in Fig. 3 and compared with that from the tensile test at RD. Hereby, the Swift equation is given by Eq. (21)

$$\bar{\sigma} = K\left(\bar{\varepsilon}_0 + \bar{\varepsilon}_p\right)^n \tag{21}$$

Fig. 2 Schematic of the hydraulic bulge test

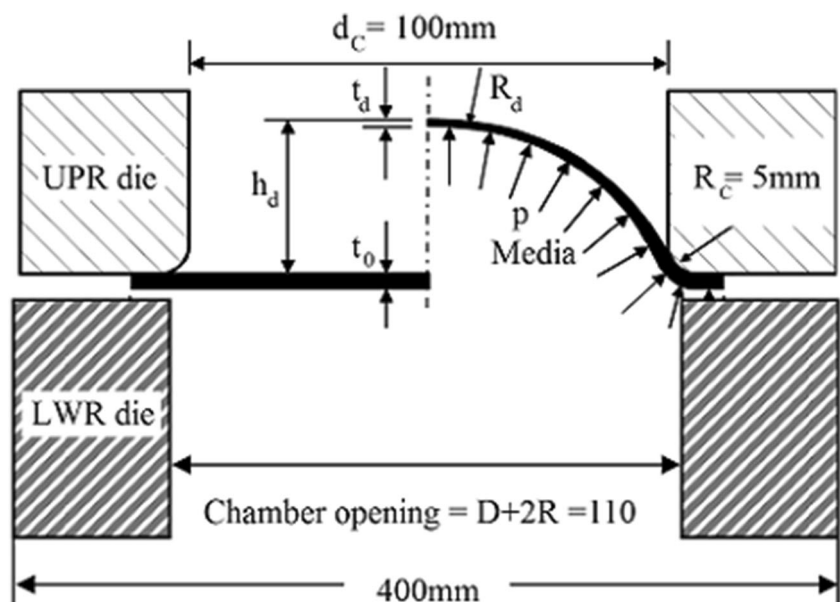


Table 4 Determined material constants of the Swift hardening model for the investigated aluminum sheet grade AA5052-H32

k (MPa)	ε_0 (-)	n (-)
343.58	0.0054	0.1098

where $\bar{\varepsilon}_p$ denotes the equivalent plastic strain, K is the strength coefficient, n is the strain hardening exponent and ε_0 is the material constant of the Swift function. The Swift model parameters were obtained for the examined sheet, as shown in Table 4. It is worth noted that the strain hardening exponent n of 0.1098 was close to the uniform elongation in Table 2, as also reported in Bandstra and Koss [52]. Obviously, the Swift law exhibited a good approximation of the strain hardening behavior of concerned material. Otherwise, the bulge test provided the experimental stress-strain curve with much larger strain than the tensile test. As a result, the aluminum sheet achieved the maximum strain of 0.15 and 0.34 under uniaxial tension and biaxial tension states, respectively. The flow stress curves of bulge test were noticeably higher than those of tensile tests in all directions. Finally, the normalized flow stress at balanced biaxial stress state was also calculated, as given in Table 3.

3.3 Disk compression test

The disc compression test was aimed to characterize the anisotropy of aluminum sheet under the balanced biaxial condition. The compression test was carried out on a universal testing machine, in which the experimental procedure was well described in Kuwabara et al. [53]. First, circular disk specimens with the diameter of 10 mm were prepared by an

electrical discharge machining. In this work, the initial compressive load of 10.5 kN was employed and the load was increased stepwise 0.25 kN per test. For each load condition, three repeated samples were used. To minimize the effects of friction, lubricant oil was regularly applied to the sample surfaces. After each compression, sample diameters were measured along the rolling and the transverse direction and the plastic true strains in both directions (ε_{RD} and ε_{TD}) were then calculated according to Eq. (22).

$$\varepsilon_{RD} = \ln(D_{RD}/D_{RD}^0), \varepsilon_{TD} = \ln(D_{TD}/D_{TD}^0) \quad (22)$$

where D_{RD}^0 and D_{TD}^0 are the initial diameters of the samples in the RD and TD, respectively. The plastic true strains ε_{RD} and ε_{TD} in the rolling and transverse directions were plotted and fitted by using a linear regression, as depicted in Fig. 4. Then, the balanced biaxial r_b value of 0.9586 was gathered from this relationship with respect to Eq. (23)

$$r_b = \frac{d\varepsilon_{TD}}{d\varepsilon_{RD}} \quad (23)$$

3.4 Anisotropic yield and hardening parameters

To determine the anisotropic material parameters of the Hill'48 and Yld2000-2d yield criteria, the yield stresses and the r -values determined from different loading conditions were used. In the case of Hill'48 model, all model parameters were identified by means of Eq. (14) along with the r -values from the tensile tests. Table 5 shows the calculated anisotropic coefficients of the Hill'48 function for the examined aluminum sheet. On the other hand, the anisotropic parameters of the Yld2000-2d criterion needed to be computed through a numerical iteration method. Hereby, two additional stress and strain values of the biaxial state from the hydraulic bulge test and disk compression

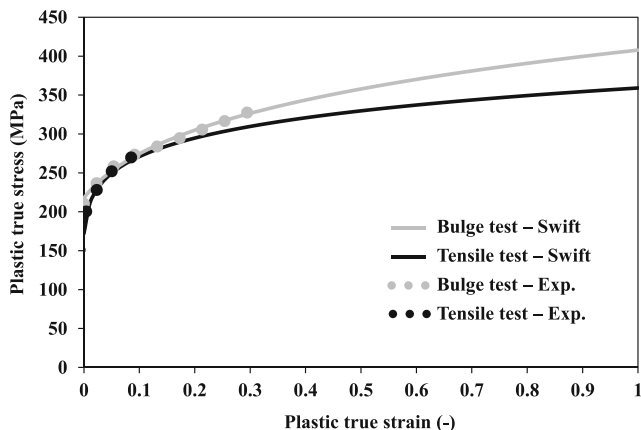


Fig. 3 Flow stress curves experimentally obtained from the bulge test and tensile test and extrapolated using the Swift law

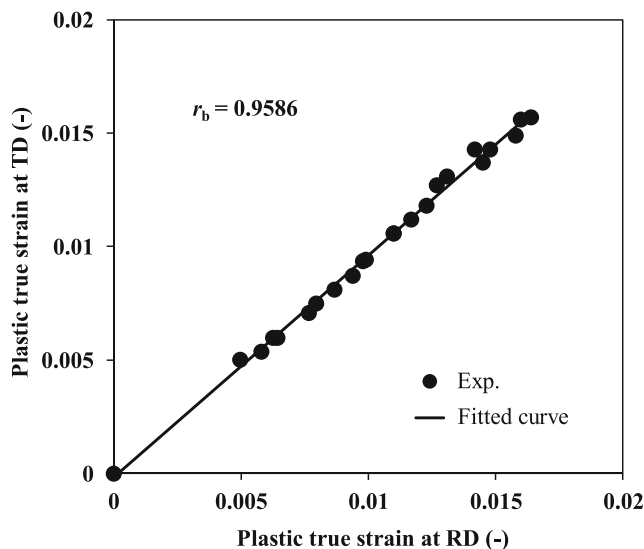


Fig. 4 Relationship between plastic true strains in the RD and TD of the investigated aluminum sheet determined from the disk compression test

test, respectively, were applied. It is noted that the crystallographic-dependent parameter M of 8 for FCC alloy was given here. The obtained material constants of the Yld2000-2d model are summarized in Table 6.

Moreover, the normalized flow stresses and r -values were numerically calculated by using the Hill'48 and Yld2000-2d yield functions. The predicted and experimental results of both values are compared in Fig. 5(a) for all test directions. It was typically found that the flow stresses as well as r -values in all directions obtained by the Yld2000-2d model agreed well with the experimental data. In contrast, the Hill'48 model could accurately describe the r -values in all directions, while its predicted flow stresses in the DD and TD showed large deviations. It is noticed that both yield stresses and r -values of the investigated sheet in the DD and TD were higher than those in the RD. Figure 5(b) illustrates the yield loci or the relationships between normalized TD and RD stresses predicted by the used yield criteria in comparison with the experimental results of tensile tests. It is seen that the Yld2000-2d model correctly represented the experimental stress pairs at all given stress states. Nevertheless, the Hill'48 model could only predict the result of uniaxial tension state at the RD, but underestimated and overestimated the yield stresses under biaxial tension and uniaxial tension at the TD, respectively.

Table 5 Determined anisotropic coefficients of the Hill'48 model (r -value based) for the investigated aluminum sheet grade AA5052-H32

F	G	H	N
0.4648	0.6044	0.3956	1.3567

Table 6 Calculated anisotropic coefficients of the Yld2000-2d model for the investigated aluminum sheet grade AA5052-H32

α_1	α_2	α_3	α_4	α_5	α_6	α_7	α_8
0.889164	0.995898	0.861674	0.923236	0.964497	0.711258	0.965602	1.125148

4 Experimental determination of critical fracture strains

It was aimed in this work to develop anisotropic fracture locus of the aluminum sheet grade AA5052-H32 through experimental and numerical calculation approaches. Therefore, critical plastic strains at fracture of investigated sheet for the entire range of stress state were initially determined. Tensile tests of samples with various notches and geometries and Marciniak in-plane stretch forming tests were performed for different three material orientations. During the experiments, an optical strain measurement with the DIC technique were performed to precisely identify critical sites and corresponding strains at a state shortly before fracture of each deformed sample. The details of the experiments are given in following.

4.1 Tensile test of specimens with varied geometries

In this work, the critical strains at fracture onset of the investigated AA5052-H32 sheet for the stress states in the left-hand side of forming limit diagram were determined by means of tensile tests of sheet specimens with different geometries. The varying notches and geometries of tensile samples were applied in order to achieve different strain paths from pure shear to plane strain deformation states, as shown in Fig. 6. Tensile tests were conducted for all sheet specimens with a crosshead speed of 0.1 mm/min. During the tests, strain histories and critical strains at the onset of fracture on specimen surface were gathered by the DIC technique, as illustrated in Fig. 7(a). The six tensile specimens in Fig. 6 are called pure shear sample (1), combined loading sample (2), uniaxial tension samples (3 and 4) and plane strain samples (5 and 6). In an in-plane condition, the pure shear and combined loading sample provided the strain ratio between -1 and -0.5, while the uniaxial tension and plane strain samples allowed the strain ratio from -0.5 to 0. All specimen types were prepared along three orientations of sheet (RD, DD and TD) for examining the anisotropy effect on the fracture onset strain. From the measured strain distributions before fracture of the critical locations on each sample, as depicted in Fig. 8, the maximum strains for fracture initiation including their strain paths could be precisely determined for all specimens. These identified critical strains from different loading directions were further used to construct the FLs of the examined sheet.

4.2 Marciniak in-plane stretch forming test

To obtain the fracture strains of the investigated aluminum sheet grade AA5052-H32 for the states of stress in the right-hand side of forming limit diagram a modified Marciniak in-plane forming test was carried out on a universal testing machine MTS 810, as shown in Fig. 7(b). The detailed geometries of tools installed in this experiment are given in Fig. 9(a). Hereby, the flat bottom cylindrical punch had a diameter of 50 mm. The radii of upper die and punch shoulder were 3 mm and 10 mm, respectively. A recessed area in the middle of the punch was applied for minimizing the friction between punch and blank. In addition, for the same purpose, a 1 mm thick and 100x100 mm² aluminum washer including a circular hole of the diameter of 11 mm was inserted between punch and sheet and a lubricant oil grade SAE 40 was applied on the washer surface in contact with the punch. It was necessary to obtain a frictional force between the two blanks much larger than that

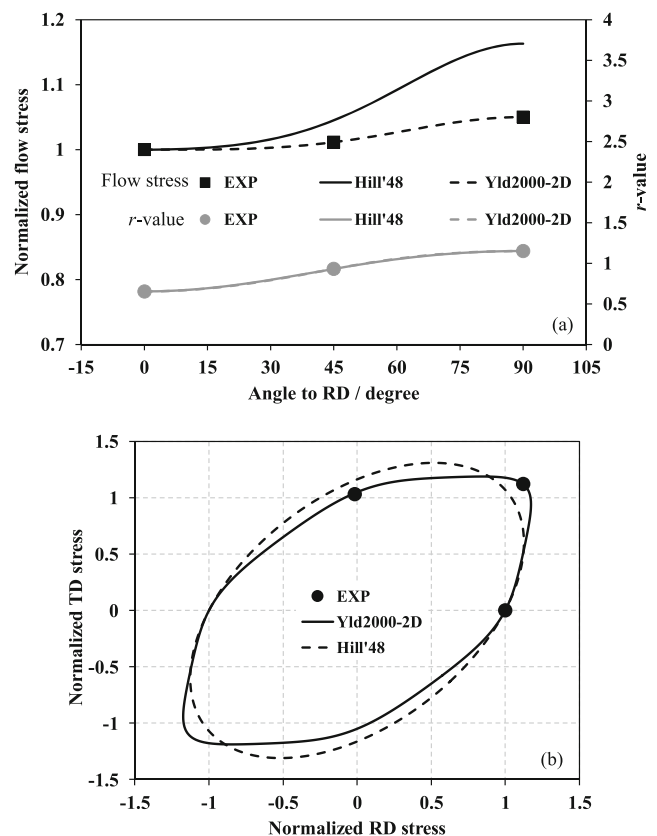


Fig. 5 (a) Normalized flow stresses, r -values and (b) yield loci experimentally determined and numerically predicted by different yield criteria for the investigated AA5052-H32 sheet in comparison

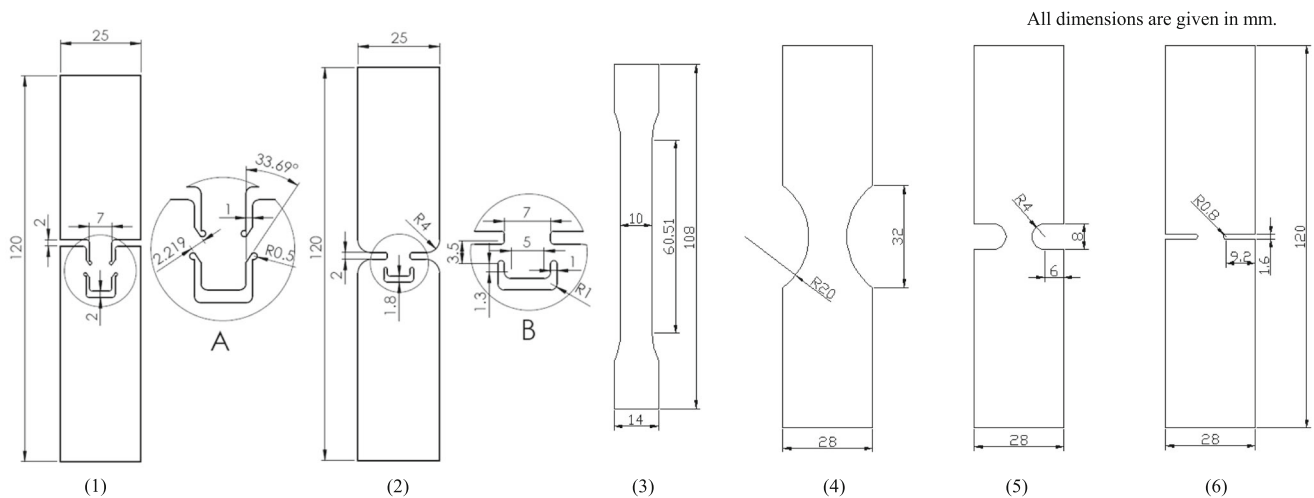


Fig. 6 Sample geometries used in tensile tests for determining the strains at fracture of the examined aluminum sheet

between punch and washer. A lock bead was used to prevent undesired material draw-in during the test. It is noted that this test setup could eliminate bending and curvature effect, which generally occurred in a conventional Nakajima stretching test, and allow a uniform material deformation throughout the entire region of interest. The dimensions of test specimens and washer are provided in Fig 9(b) and (c), respectively. These specimen geometries were similar to those used by Raghavan [54] and Quaak [55]. With the varying web widths of Marciniak test specimens, different strain paths in the positive stress state range could be generated due to a relaxation of lateral constraints. All specimen types were prepared in three different orientations.

Before the tests, 2 mm square grids were applied on specimen surfaces for a subsequent optical strain

measurement. The Marciniak tests were conducted with a constant blank holder force and constant pressing speed of 10 mm/min until fracture occurred. All samples failed after reaching a punch displacement of around 15 mm. Then, local strain distributions on the deformed samples were measured by means of the AutoGrid strain measurement system, as depicted in Fig. 10. From these results, achievable strains at fracture onset of each specimen were identified, in which fracture and necking zone in the vicinity of crack path were previously distinguished. Note that it was usually assumed that the deformations of each sheet sample in both tensile tests and Marciniak stretching tests were proportional or in other words the ratio between the principal minor strain and the principal major strain remained constant.

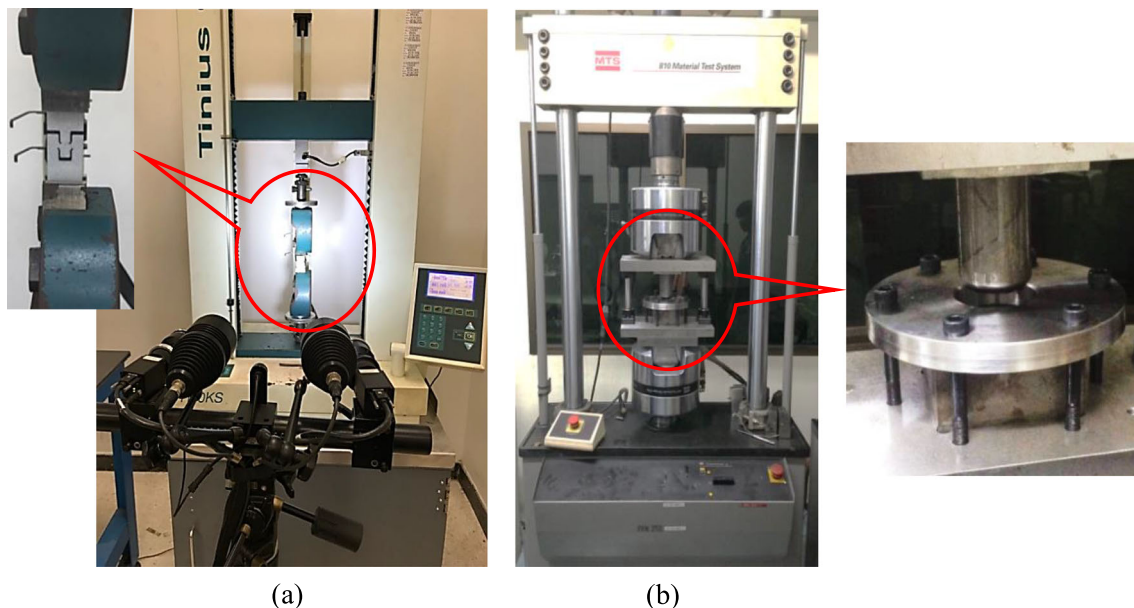


Fig. 7 Experimental test setup of (a) tensile test of specimens with varied geometries and (b) modified Marciniak in-plane stretch forming test on a universal testing machine

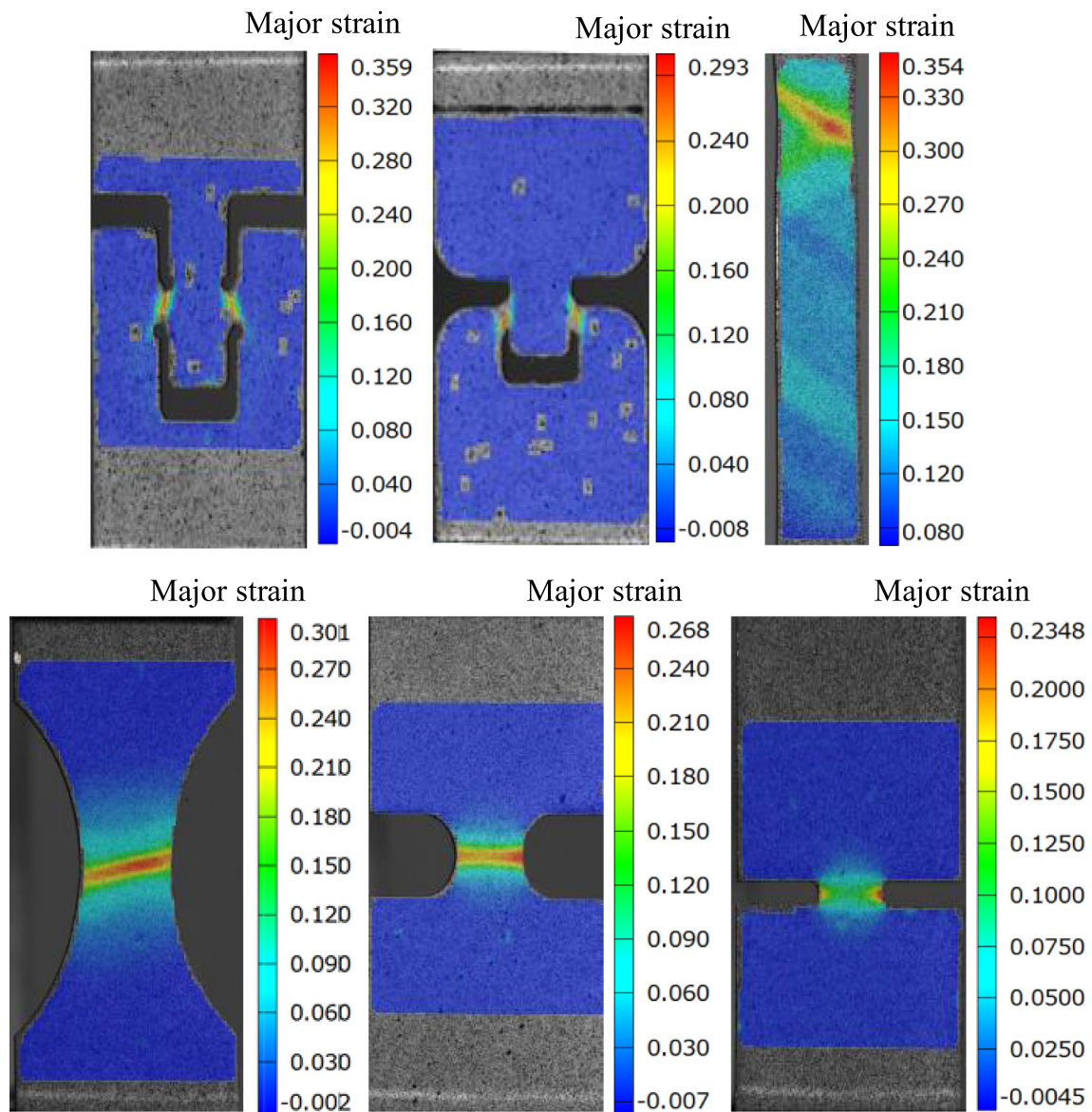


Fig. 8 Measured major strain distributions on the deformed samples of different geometries before fracture

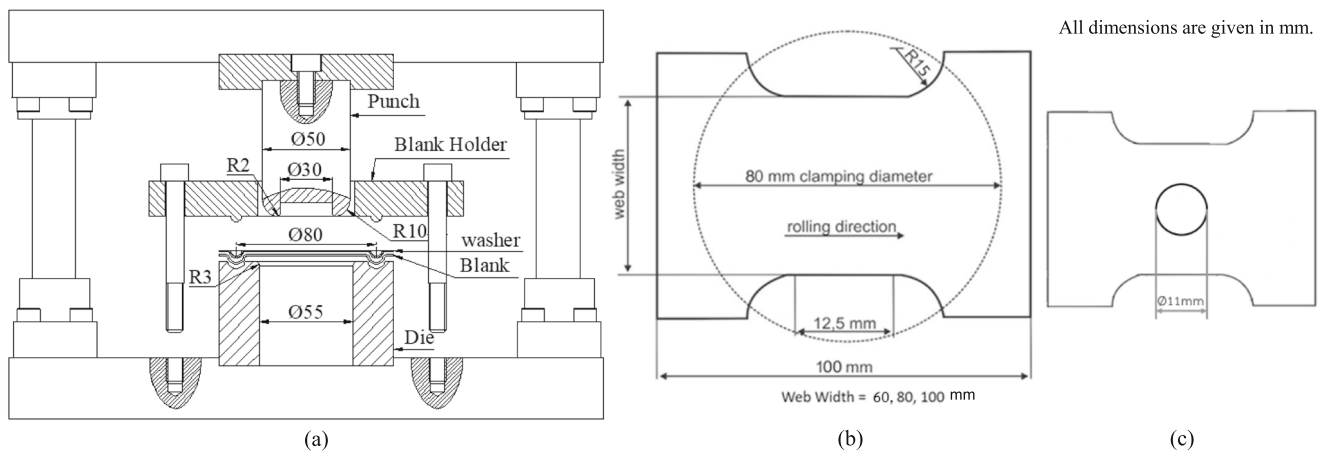


Fig. 9 Marciniak in-plane forming test: (a) die set, (b) used sample geometries and (c) washer

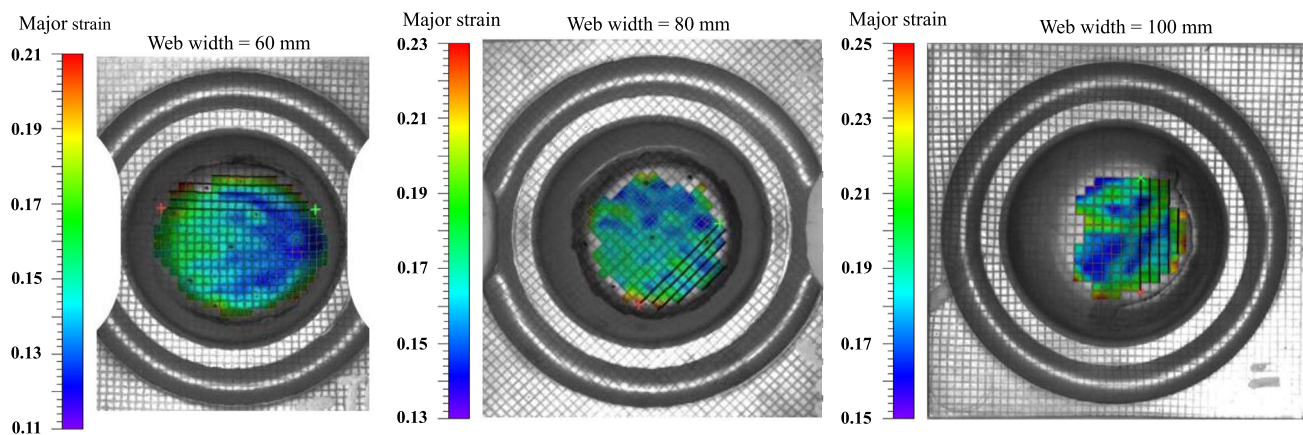


Fig. 10 Measured major strain distributions on the deformed samples from the Marciniak in-plane stretching test

5 Determined anisotropic fracture limit curve

From the results of tensile tests and modified Marciniak stretching forming tests of different sheet samples, the critical fracture strains in the entire principal strain space of the examined aluminum grade AA5052-H32 at different orientations were obtained. The Lou-Huh ductile fracture criterion was then applied for constructing the FLs with regard to the various loading directions. Firstly, the material constants C_1 , C_2 and C_3 of the fracture model were identified from the experimental fracture strain data of pure shear, uniaxial tension and plane strain samples in the tensile tests. The equivalent plastic strains to fracture were calculated under consideration of the Hill'48 and Yld2000-2d yield functions as described before. The obtained material constants of the Lou-Huh model are summarized for varying sample orientations in Table 7. By using these parameters, the stress ratio ranging from pure shear ($\alpha = -1$) until equi-biaxial tension ($\alpha = 1$) and stress triaxialities the resulting equivalent strains at fracture could be predicted with regard to each yield function and loading direction. The relationships between stress triaxiality and equivalent plastic strain to fracture were plotted as the FL for the investigated sheet by the Lou-Huh model coupled with the Hill's 48 and Yld2000-2d yield criteria in Fig. 11(a) and (b), respectively.

It is seen that the FLs obtained from the Lou-Huh model combined with both yield criteria showed noticeable discrepancies at all states of stress, since it was due to the fact that at large plastic deformation the yield function could strongly affect the resulting limit strains. In general, the Yld2000-2d model provided somewhat higher fracture thresholds than the Hill'48 model. The fracture model could well represent the anisotropy effect of material, in which the constructed FLs of three loading directions were considerably deviated in the entire stress space. However, the prediction accuracy certainly depended on the applied yield criterion. It was found that the plastic strain to fracture of sheet in the TD was lowest under the plane strain state, while in contrast it was highest under the

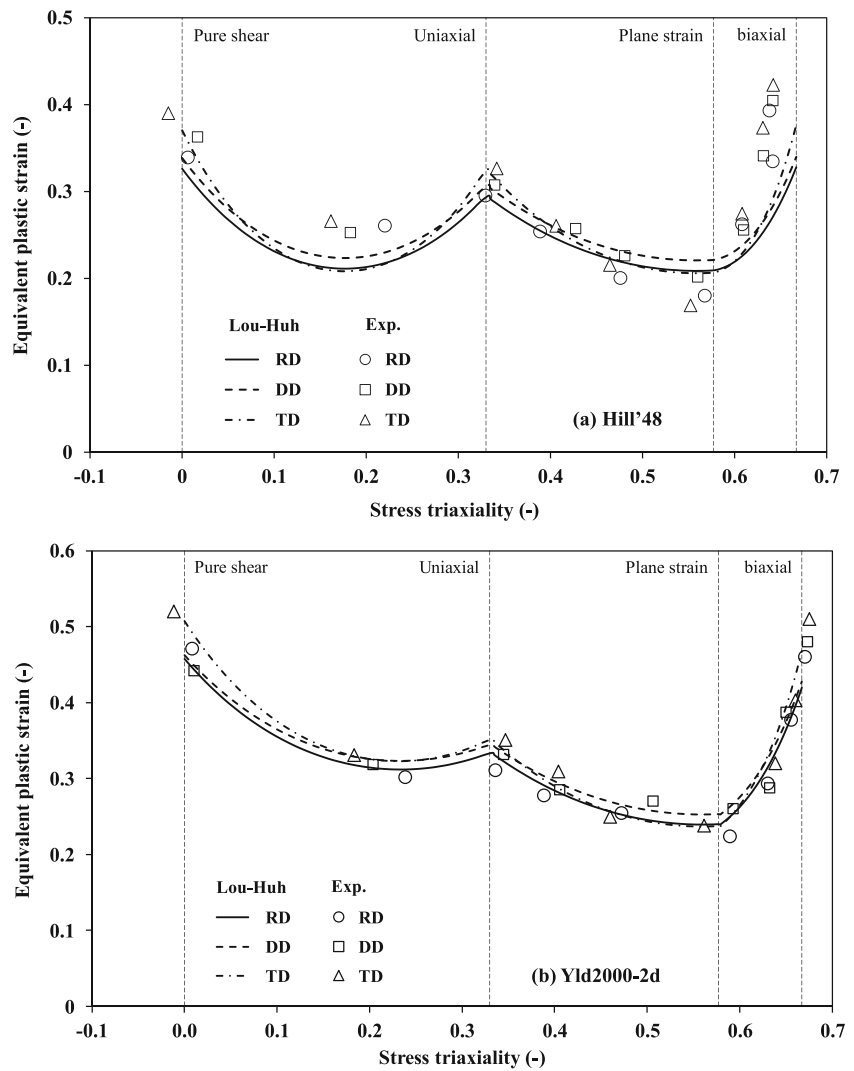
pure shear, uniaxial tension and equi-biaxial load. In the case of aluminum sheet in the DD, the largest fracture strain was observed at the plane strain state and within the region between pure shear and uniaxial tension. In the RD, the sheet exhibited the lowest limit strain at the pure shear, uniaxial tension and equi-biaxial tension. Note that the two yield functions exhibited the similar characteristic. The effect of plastic anisotropy of the investigated aluminum sheet on its fracture forming limit was significant. By the introduced approach, the fracture limit curves could be calculated in consideration of damage evolution and anisotropic behavior of material. Nevertheless, these determined FLs were later transformed to strain based fracture onset limit curves so that a formability prediction of material in sheet metal forming processes became more applicable.

For the verification of the Lou-Huh model, the predicted FLs were compared with all fracture limits determined by the tensile and Marciniak tests. The experimental fracture strains in the major and minor principal strain space were firstly converted into fracture data points of equivalent plastic strain and stress triaxiality. Hereby, the strain ratios, stress ratios and stress ratio parameters of each sheet orientation were considered with respect to both used yield criteria. Finally, the data pairs of stress triaxiality and equivalent plastic strain to fracture obtained from the experiments were obtained and plotted

Table 7 Calculated material constants of the Lou-Huh fracture criterion coupled with the Hill'48 and Yld2000-2d yield models of the investigated aluminum sheet grade AA5052-H32 in different directions

Orientation	Hill'48			Yld2000-2d		
	C_1	C_2	C_3	C_1	C_2	C_3
0° (RD)	3.3932	0.0219	0.2953	3.3599	0.0312	0.3008
45° (DD)	3.2406	0.0215	0.3076	3.1672	0.0311	0.3121
90° (TD)	4.5059	0.0197	0.3251	4.4501	0.0301	0.3290

Fig. 11 Fracture loci predicted by the Lou-Huh fracture model and obtained from the experiments coupled with (a) the Hill'48 and (b) Yld2000-2d yield function for the investigated aluminum sheet in different loading directions



for the Hill'48 and Yld2000-2d yield criterion in Fig. 11(a) and (b), respectively, along with the predicted FLs from the Lou-Huh model. Generally, it is seen that the predicted FLs coupled with both yield criteria fairly agreed with the experimental results. Nevertheless, the Lou-Huh model combined with the Yld2000-2d yield function could more precisely describe the experimental fracture data points at all stress states than that with the Hill'48 yield function. The largest discrepancy occurred at the plane strain region. It is worth noted that the observed deviations between the fracture limits of different sample orientations or the effect of material plastic anisotropy with regard to the prediction and experiment were comparable.

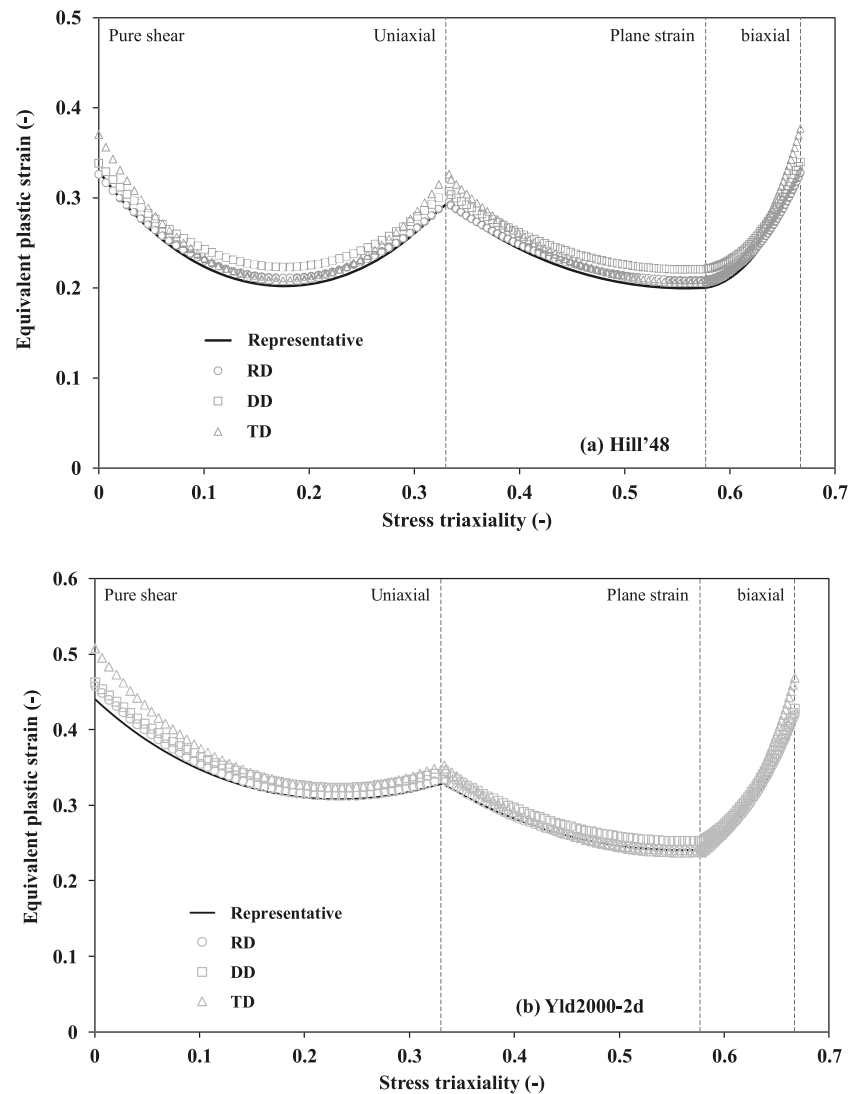
In addition, the FLs of different sample orientations were reduced to a single fracture limit curve, in which the lowest plastic strains of all three FLs at all states of stress were taken into account. By this means, the derived unique anisotropic FL from the lower bound could conservatively describe the fracture onsets of material under all loading directions. For

this purpose, the material constants of the Lou-Huh model C_1 , C_2 and C_3 were initially identified by using the lowest equivalent plastic strains to fracture among the data of all three directions from the pure shear, uniaxial tension and plane strain conditions. The material model parameters obtained by coupling with the Hill'48 and Yld2000-2d yield functions are given in Table 8. Then, the representative FL of the examined aluminum sheet was generated according the Lou-Huh criterion. The anisotropic FLs, which represented the FLs of

Table 8 Determined material constants of the Lou-Huh fracture criterion coupled with the Hill'48 and Yld2000-2d yield functions for constructing the representative anisotropic FL

	Hill'48		Yld2000-2d		
	C_2	C_3	C_1	C_2	C_3
C_1	0.0219	0.2953	3.8259	0.0312	0.3008

Fig. 12 Representative anisotropic FLs of the examined aluminum sheet predicted by the Lou-Huh model using (a) the Hill'48 and (b) Yld2000-2d yield criterion



all loading directions and predicted by the fracture model combined with the Hill'48 and Yld2000-2d yield criterion, are illustrated in Fig. 12(a) and (b), respectively.

The proposed anisotropic FLs were also transformed into the strain-based FFLC, which covered the entire range of concerned state of stress and could be directly applied in a sheet metal forming analysis, similar to those works in Beese et al. [56] and others [34, 35, 39–41]. Hereby, the construction of FFLC was done on the basis of the determined equivalent plastic strains, stress ratios, strain ratios and the stress ratio parameters coupled with the Hill'48 and Yld2000-2d yield criteria. The critical equivalent plastic strains of the FLs based on the Lou-Huh model were transformed into the principal strain space by means of Eqs. (10) and (6). The anisotropic characteristics of examined aluminum sheet were taken into account by the stress ratio parameters (ξ), which were calculated with regard to each yield function. The obtained representative FFLCs of the investigated aluminum sheet in all

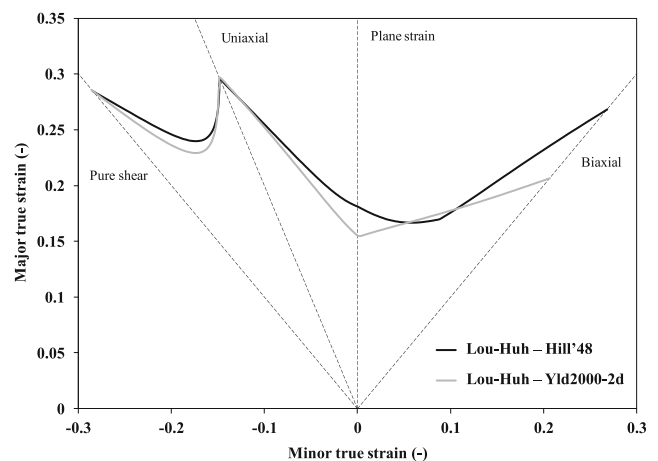


Fig. 13 Representative anisotropic FFLCs of the examined aluminum sheet transformed from the FL based on Lou-Huh fracture model coupled with the (a) Hill'48 and (b) Yld2000-2d yield criterion

loading directions by using both yield functions are depicted in Fig. 13.

6 Verification

In order to verify the determined anisotropic forming limit curves of the investigated aluminum sheet grade AA5052-H32, two experimental forming tests, namely, cross die forming and square cup drawing tests were used. FE simulations of both forming experiments were subsequently conducted and resulted formabilities of deformed parts were studied by means of the predicted FFLCs. Hereby, the accuracies of the FFLCs could be evaluated and discussed. It is noted that the FFLC generated by the Lou-Huh fracture model coupled with the Yld2000-2d criterion was employed here as it more accurately described the fracture states of used sheet in the experiments.

6.1 Cross die forming test

A cross-die forming test was experimentally carried out on a universal testing machine. The dies, installation and test setup are illustrated in Fig. 14(a). Such cross-die shape was often employed to reproduce forming condition with complex strain paths in various states of stress of an industrial part. The cross-die tools consisted of a cross-shaped punch, blank holder and

lower die. The die set was designed for an initial rectangular blank size of $134 \times 134 \text{ mm}^2$, a clearance of 2.6 mm and a punch stroke of 60 mm. In this work, sheet samples for the cross-die test were additionally positioned in both RD and DD in order to examine the effects of sample orientation, as depicted in Fig. 14(b). The blank holder force of about 16.5 kN and lubricant oil grade SAE 40 were applied. During the tests, the samples were pressed until a first crack appeared. Concurrently, FE simulations of the cross-die test were conducted in ABAQUS/implicit with a symmetry condition, as seen in Fig. 14(c). The boundary conditions were given corresponding to the experiment. The punch, die, and blank holder were defined as a discrete rigid body with the mesh size of $2 \times 2 \text{ mm}^2$. The square blank sheet was discretized with four-node quadrilateral shell elements (S4R) and with five element layers through the thickness. The smallest mesh size of 1 mm was used, for which the mesh sensitivity was studied in previous studies. The Coulomb’s friction coefficient of 0.075 was employed for all contact pairs. This value was close to the values in many works, where aluminum sheets were examined [57]. On the other hand, FE simulation using different friction coefficients were performed and the results from this value agreed well with the experimental ones. Furthermore, in the simulations, the material anisotropy and strain hardening behavior were described by the Hill’48 and Yld2000-2d yield criteria and Swift hardening law, respectively. These yield criteria and hardening model were successfully applied for

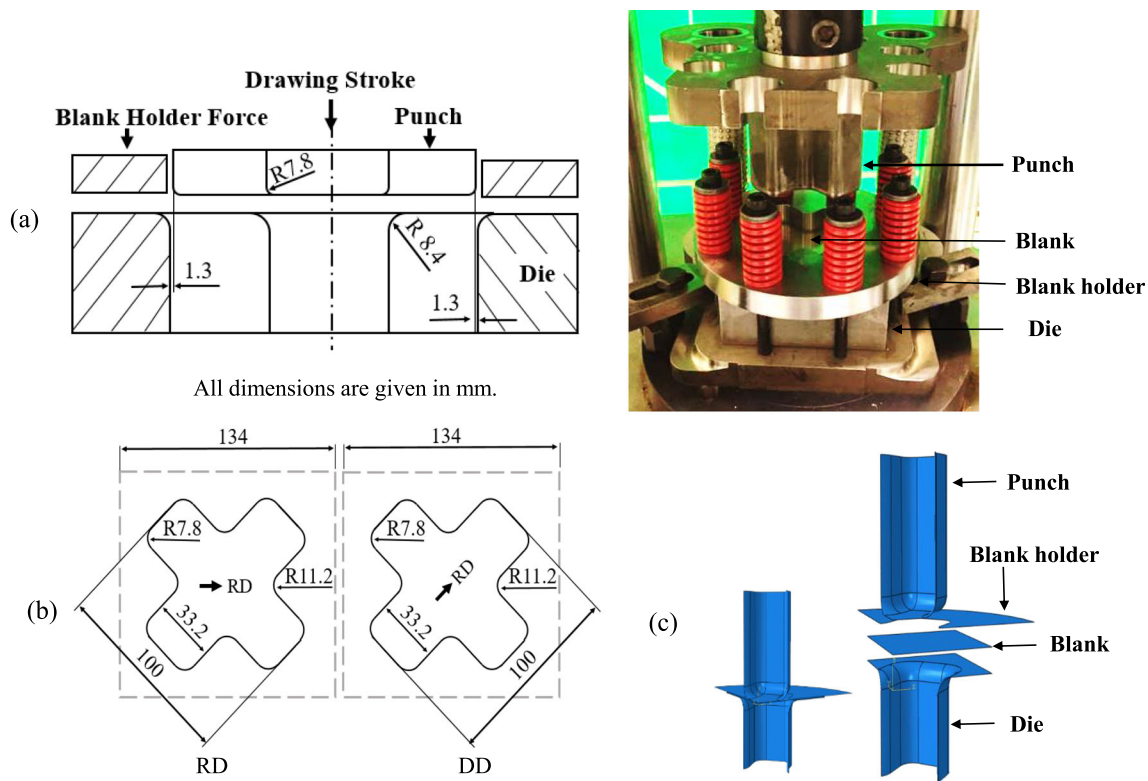


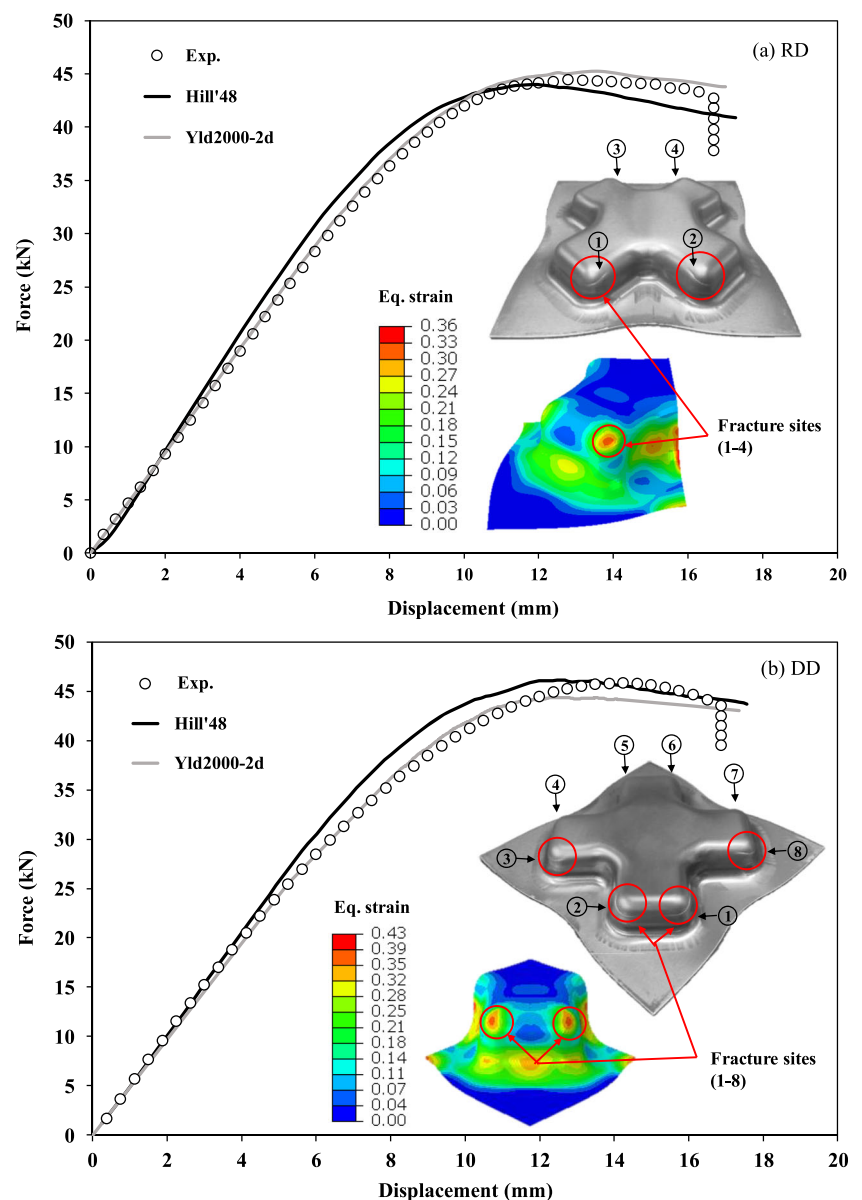
Fig. 14 Cross-die forming test: (a) experimental installation and setup, (b) sample orientation and (c) FE model

the forming analyses under plane stress state of various grades of aluminum sheets in Manopulo et al. [58] and Gorgi et al. [59, 60]. Hereby, the previously identified material parameters from Tables 4, 5, and 6 were used.

The representative anisotropic FFLCs were applied to the FE simulations of cross-die forming test with an uncoupled method for describing resulted forming limits of sheet samples. It was found that fractures of both formed samples aligned in the RD and DD basically developed around the sample edges, as illustrated in Fig. 15(a) and (b), respectively. The fractures of the RD sample were observed at the four edge radii marked in circles in Fig. 15, while the DD sample showed crack appearances at all eight corners in Fig. 15(b). These emerged cracks at the punch radii of sheets afterwards propagated in both circumferential directions. The altered sample orientations noticeably

led to different failure characteristics due to the material anisotropy. Otherwise, force-displacement curves were gathered from the experiments and compared with those predicted by the simulations, as shown in Fig. 15. The punch force-displacement curves calculated by using different yield functions exhibited a considerable deviation. However, for both cross-die samples in the RD and DD, the predicted force-displacement curves until fracture from the Yld2000-2d model were more accurate than those based on the Hill'48 model when comparing with the experimental results. Note that the declines of experimental curves could not be calculated since no fracture criterion was coupled in the simulations. In general, it is seen that the fracture sites and their propagations predicted by the FFLC agreed well with those found in the experiments for both sample directions.

Fig. 15 Force-displacement curves and samples at failure determined from the experiment and predicted by FE simulation of the cross-die forming test in the (a) RD and (b) DD in comparison



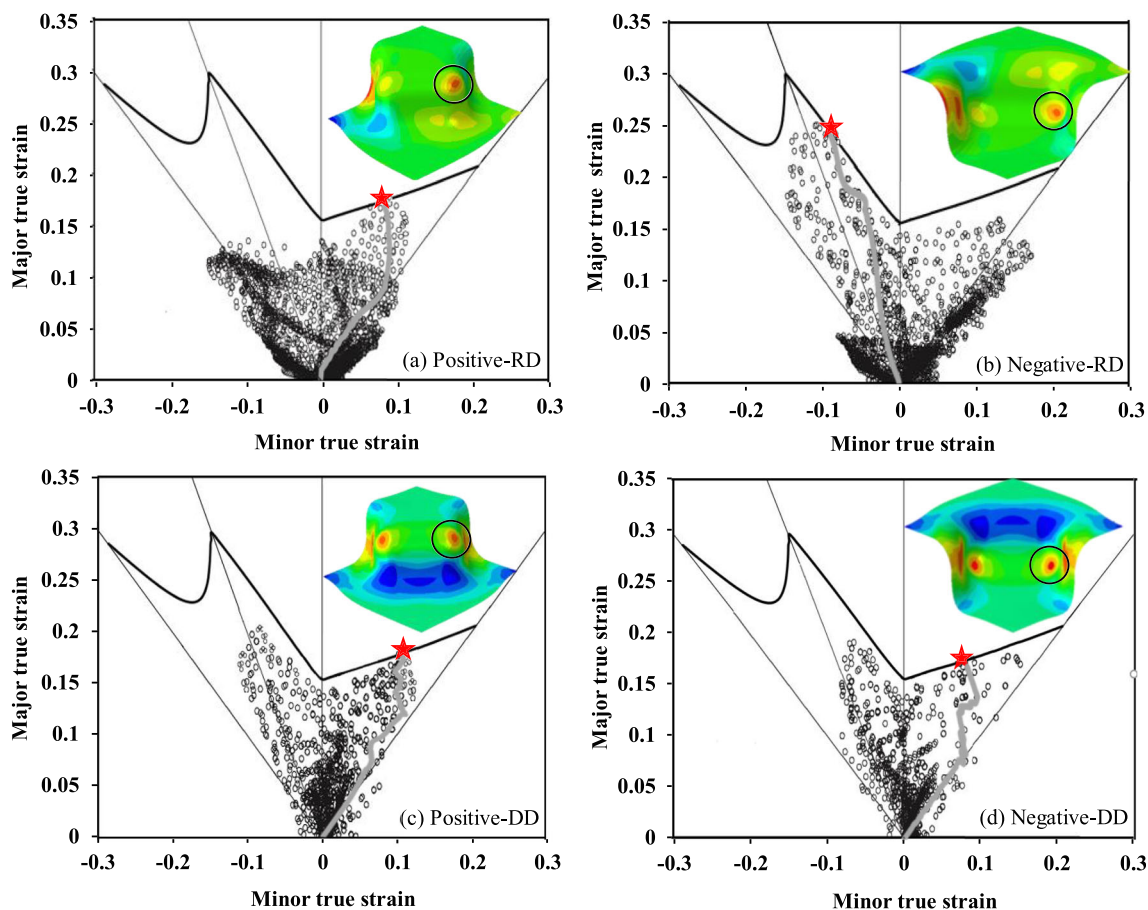


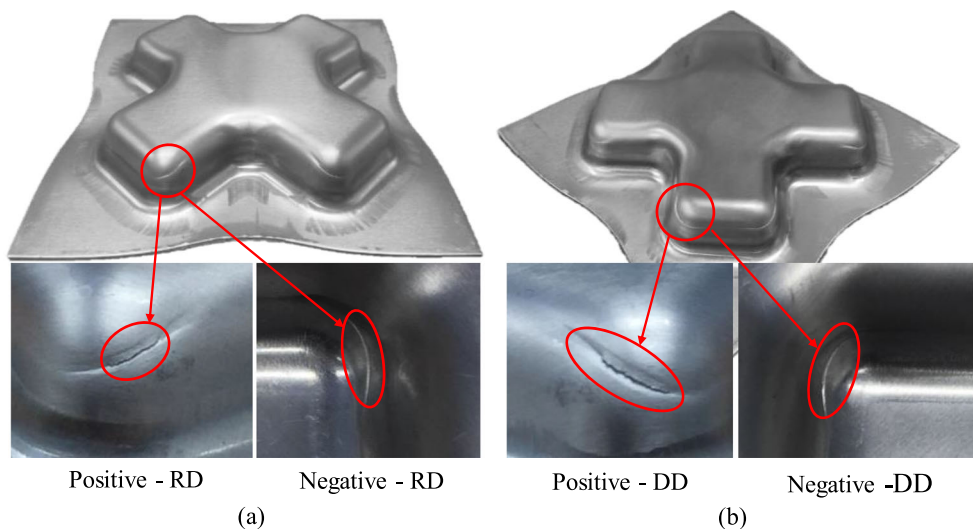
Fig. 16 Calculated local strain distributions on the (a) positive surface, (b) negative surface of the RD sample and (c) positive surface, (d) negative surface of the DD sample at the experimental fracture states in

the cross-die forming test along with the strain path of the critical site until fracture and the anisotropic FFLC

In addition, from the simulations, local major and minor principal strains at failure were gathered for the crack initiating areas of deformed samples in both RD and DD. Then, the calculated strain pairs on the inner (negative) and outer (positive) surfaces of sheet samples at the moments of fracture

observed in the experiments were plotted on the determined FFLCs, as demonstrated in Fig. 16. The computed strain path of the critical site up to fracture was also given for each cases along with the strain distributions of failed samples, where predicted fracture areas could be noticed. The star symbols

Fig. 17 Fractures on the inner and outer surfaces of failed aluminum sheet samples from the cross die forming test in the (a) RD and (b) DD



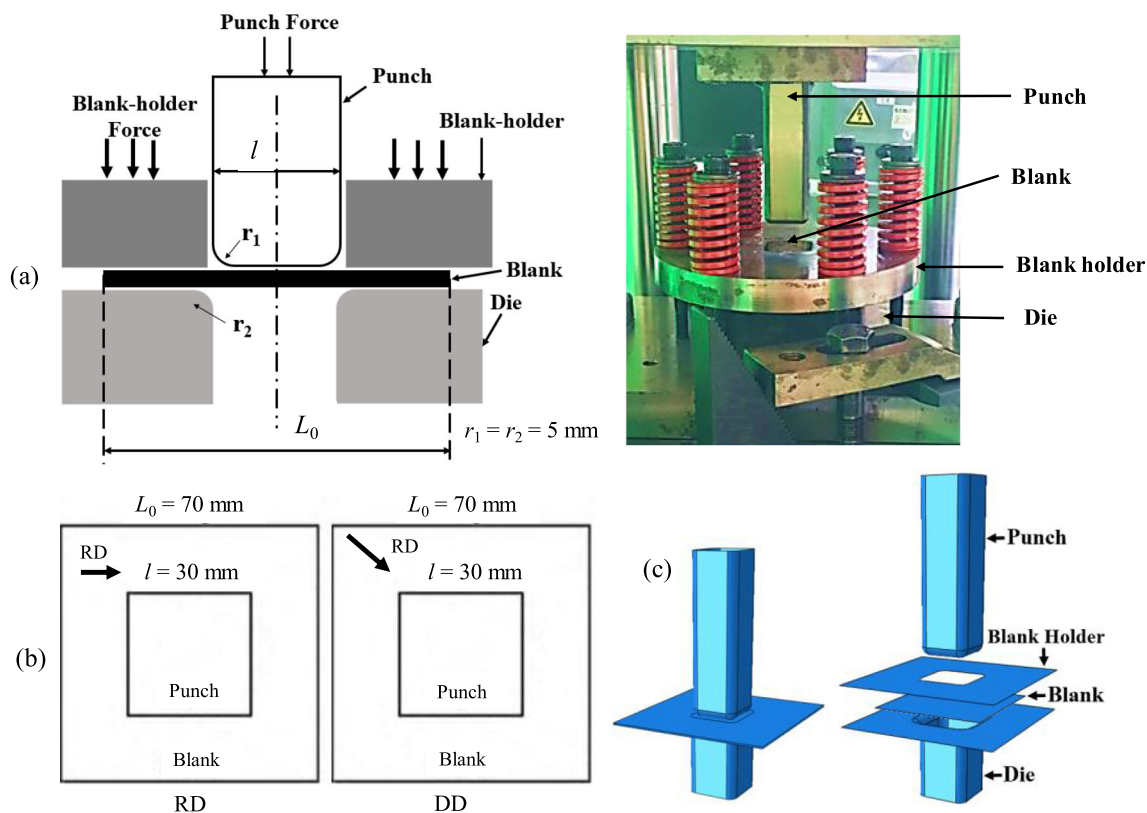


Fig. 18 Square cup drawing test: (a) experimental installation and setup, (b) sample orientation, and (c) FE model

on the strain paths showed the moments when total failure of the corresponding samples occurred. It is noteworthy that the cross-die samples were subjected to a complex plastic deformation, which incorporated a wide range of stress states ranging between uniaxial, plane strain and biaxial conditions. The crack initiation on the positive surface of RD sample at the corners was accurately described by the FFLC, since the maximum strain pairs just exceeded the given FFLC at the biaxial tension region in Fig. 16(a). On the other hand, the fracture appeared on the negative surface of RD sample because of the uniaxial tension, as seen in Fig. 16(b). Regarding a bending effect, some result differences of the top and bottom surfaces of sheet samples were obtained, similar to those reported in Li et al. [34] and Habibi et al. [61]. In the case of DD sample, the distributions of principal strain pairs on both surfaces were also provided along with the FFLC in order to investigate the influence of material anisotropy. Obviously, the proposed FFLC could fairly predict failure characteristics of both positive and negative surface of the DD sample. However, the fracture onsets of DD sample were governed only by the biaxial tension. The representative FFLC with consideration of material anisotropy could correctly describe the failure states and fracture locations of samples during the cross-die forming test under different sample orientations. Figure 17 depicts the RD and DD samples at failure from the experiments with the fracture appearances on the positive and negative surfaces respectively. It can be seen that fracture initiation was

triggered first on the outer surface of the cross-die samples as the size of fracture zones and crack depth at the corners on the outer surface were considerably larger than those on the inner surface.

6.2 Square cup drawing test

Another laboratory application for verification of the proposed FFLC was a square cup drawing test, in which states of stress between -1 and -0.5 due to the drawing process were generated that could result in a typical fracture under shear stress state. The experimental square cup drawing test was performed on a universal testing machine and its schematic installation and test set up are illustrated in Fig. 18(a). The drawing tool consisted of a square-shaped punch, blank holder and lower die. The punch had a rectangular cross section of 30×30 mm² and the same punch and die radii of 5 mm was used. The blank sheet had also a square shape of the cross section of 70×70 mm². As the cross die forming test, the test sheets were aligned in two orientations, namely, in the RD and DD, as shown in Fig. 18(b). A constant blank holder force of about 4.5 kN was kept and the lubricant oil grade SAE 40 was also used. During the experiments, sheet samples were pressed until a first crack occurred at the draw depth of around 15 mm. FE simulations of the square cup drawing tests were simultaneously carried out with consideration of the FFLC in an uncoupled way, as shown in Fig. 18(c). The boundary

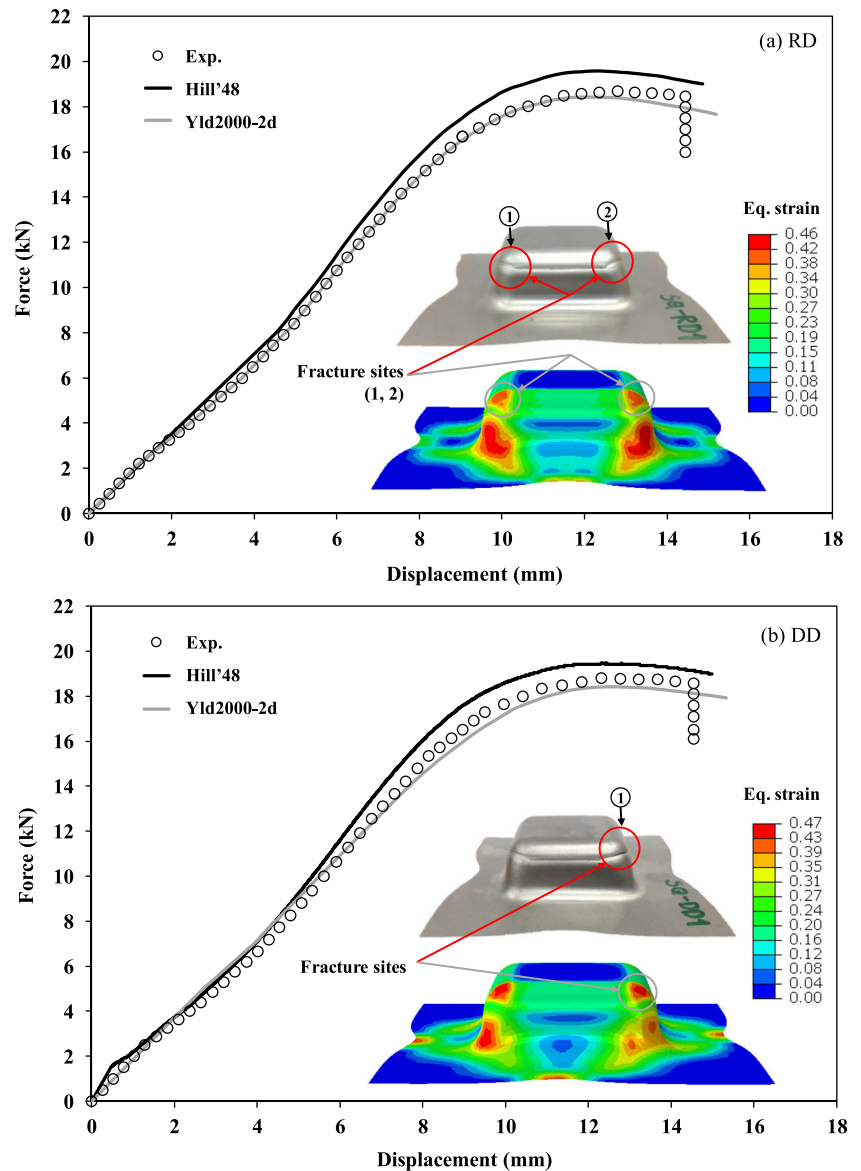
conditions in the simulations were given as in the experiment. The modeling and used mesh sizes of punch, die, blank holder and sheet sample were similar to those of the cross die forming test. The friction coefficient of 0.075 was applied for all contact pairs. The material anisotropic and strain hardening characteristics of aluminum sheets in the simulations were represented by the Hill'48 and Yld2000-2d yield criteria and Swift hardening law, accordingly.

Firstly, punch force-displacement curves gathered from the experiments and calculated by the FE simulations are compared in Fig. 19(a) and (b) for the samples positioned in the RD and DD, respectively. Noticeable deviations between the force-displacement curves obtained by the different yield criteria were found, in particular at large punch displacement. Nevertheless, the Yld2000-2s function could more precisely predict the experimental resulted curves of both sample

orientations than the Hill'48 model. It was observed that fracture onset and final fractures of both failed samples took place close to the punch radii, while the simulations exhibited significantly high plastic strains on the same areas. Such result was also reported in [34, 62], in which the similar forming tests were carried out. The number of severe fractures at the corners of RD and DD samples were different due to the effect of material anisotropy that was correctly represented by the simulations. Note that the results were confirmed by at least three repeated tests.

Moreover, from the simulations, local major and minor principal strains at failure were determined for the crack initiating regions of drawn sheet samples positioned along the RD and DD. Then, the determined strain pairs of the negative and positive surfaces at the fracture moments in the experiments are plotted along with the introduced FFLC, as shown in Fig.

Fig. 19 Force-displacement curves and samples at failure determined from the experiments and predicted by FE simulation of the square cup drawing test in the (a) RD and (b) DD in comparison



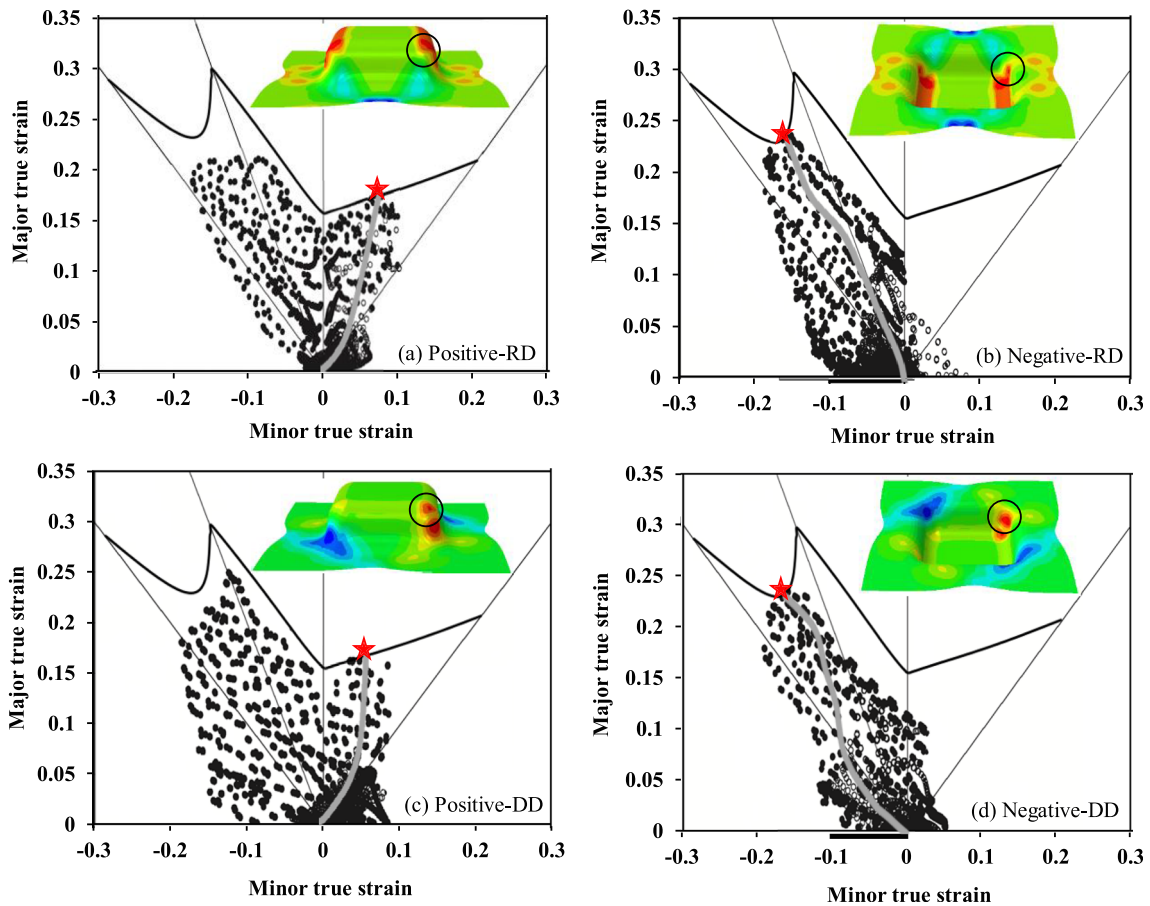


Fig. 20 Calculated local strain distributions on the (a) positive surface, (b) negative surface of the RD sample and (c) positive surface, (d) negative surface of the DD sample at the experimental fracture states in

the square cup drawing test along with the strain path of the critical site until fracture and the anisotropic FFLC

20. The calculated strain path of the critical element was also provided until fracture for each cases as well as the strain distributions of failed samples, where predicted fracture sites could be observed. The star symbols at the end of the strain paths represented the moments when total failure of the

corresponding samples took place. By the square cup drawing test, the critical strains pairs at fracture for the negative surface of both RD and DD samples exceeded the representative FFLC in the shear strain region, as seen in Fig. 20(b) and (d). On the other hand, the strain paths from the positive

Fig. 21 Triaxiality vs. equivalent strain paths of five different areas on the DD samples during the cross die forming test until experimental failure calculated by FE simulations along with the determined anisotropic FL of the examined aluminum sheet

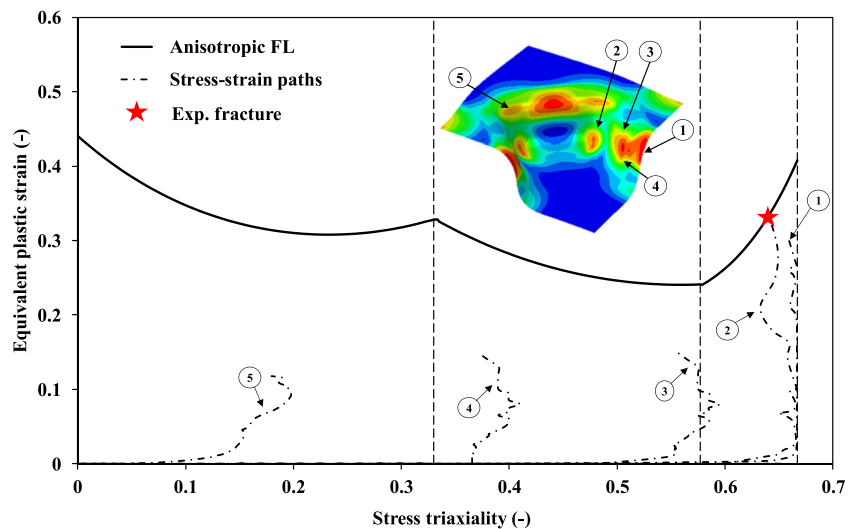
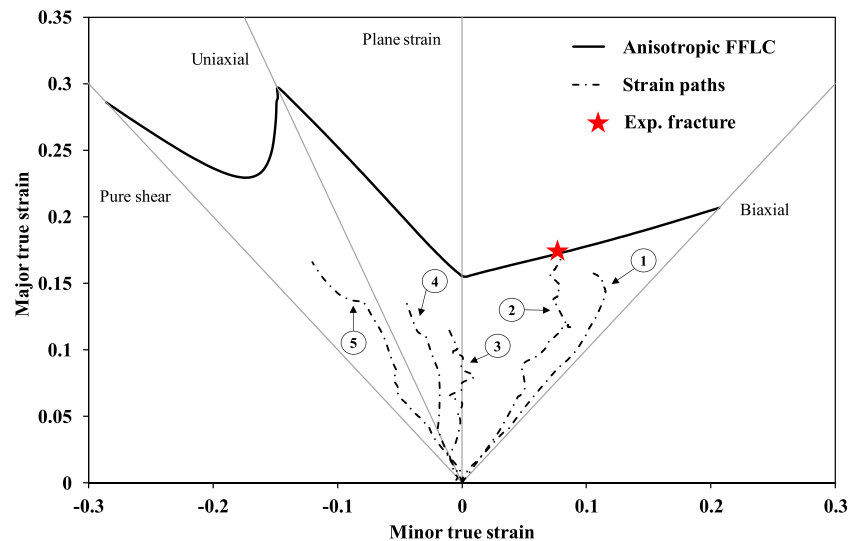


Fig. 22 Strain histories of five different areas on the DD samples during the cross die forming test until experimental failure calculated by FE simulations along with the determined anisotropic FL of the examined aluminum sheet



surface of both samples reached the FFLC in the biaxial tension zone. It is noticed that the positive surface of samples exhibited plastic deformation within almost the entire state of stress including shear, uniaxial, plane strain and biaxial tension. On the other hand, the negative surface of samples was mainly subjected to the negative stress states ranging between shear and plane strain regions. The onset of fracture was predicted on the inner surface of RD and DD sheet samples where the shear stress state generally governed that was in accordance with the observed experimental fracture appearance. The representative anisotropic FFLC could also fairly describe the failure moment of fracture of the investigated aluminum sheet grade 5052-H32 in the square cup drawing test for different sample orientations.

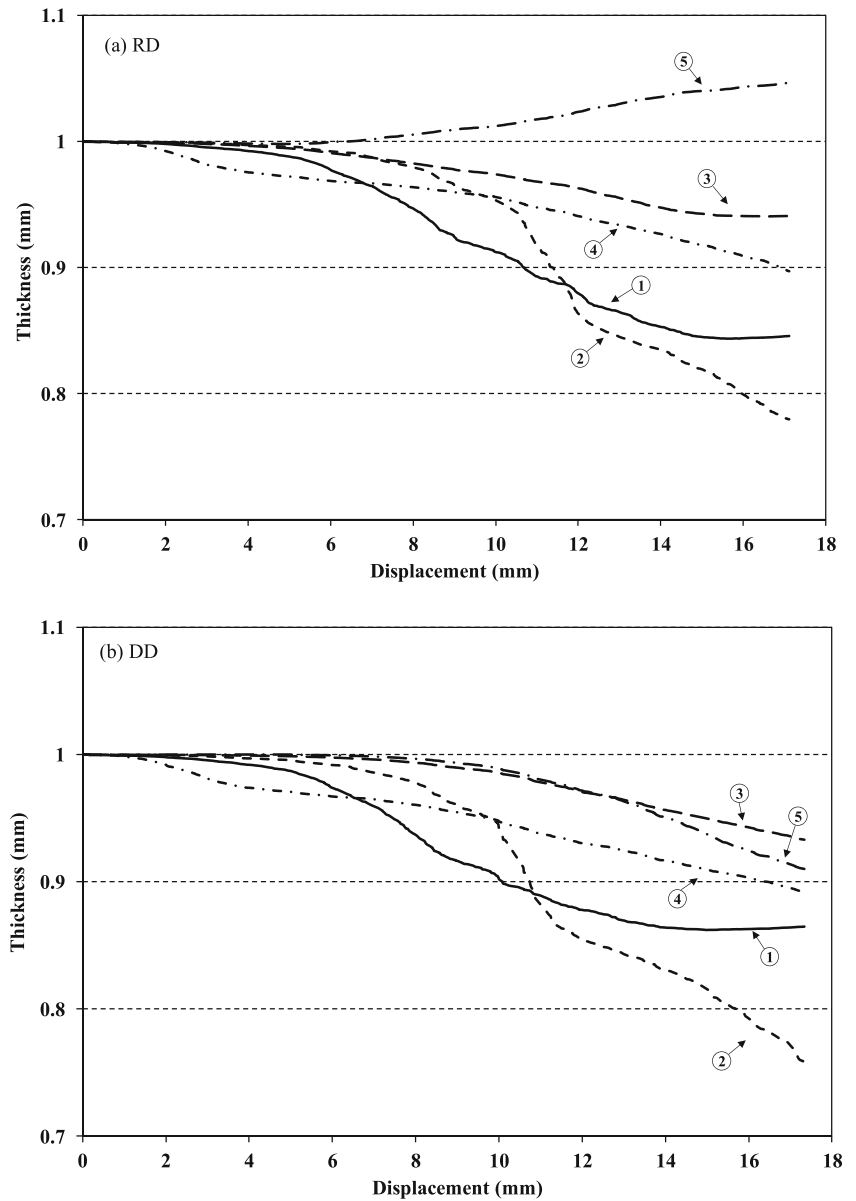
7 Forming analyses of the cross die forming test

The FE simulations and proposed anisotropic FFLC for the examined aluminum sheet grade AA5052-H32 were successfully validated in the previous section. Afterwards, the cross die forming test was further investigated in details with regard to the local stress and strain path developments, thinning and achievable drawing depths of the sampled oriented in the RD and DD in comparison. The relationship paths of calculated equivalent plastic strains and stress triaxiality for five different areas of deformed samples in the DD were determined until the experimental fracture state and compared with the representative FL, as illustrated in Fig. 21. These chosen areas were subjected to various loading conditions. Note that the positive surface was hereby taken into account. Due to the bending effect of formed sheet, its inner layer was loaded under compression, while its corresponding outer layer was loaded under tension. Therefore, the outer surface was more critical and

susceptible to fracture. The constructed FL based on the Lou-Huh criterion coupled with the Yld2000-2d could correctly predict the failures of samples positioned in both directions. The fracture occurred around the punch radius of samples, since the stress-strain history of the corresponding most critical area terminated at the FL border. The first area at the edge of sample showed rather high plastic strain in the equibiaxial stress state of the tangential and radial direction. The second area near the punch radius of sheet was subjected to a mixture of equibiaxial and biaxial tension and finally reached the FL threshold strain. This result was in agreement with the experimental observation. The third area on the side wall close to die radius exhibited much lower plastic strain in the plane strain and biaxial loading states. On the other hand, the fourth area on the side wall in the vicinity of punch radius experienced a combined uniaxial tension and plane strain state. The fifth area at the flange near the die radius was deformed by an in-plane shear stress which thereafter aimed the plane strain tension. The achieved equivalent plastic strains of the last three zones were small as compared with the limit strains of the given FL so that no fracture emerged within these areas. It is noticed that individual calculated stress-strain paths for these five different regions of the RD sample were consistent with those curves of the DD samples depicted in Fig. 21.

Furthermore, strain paths of the calculated major and minor strains were gathered until the experimental failure for the same above-mentioned areas of the DD samples on the outer surface. The obtained loading paths are compared with the representative FFLC in Fig. 22. During the cross die test, these five locations of samples sustained different forming conditions and thus a wide range of strain histories. Obviously, the strain path of the second area attained the proposed FFLC within a biaxial state of stress. It implies that the location close to the punch radius of sheet was the most critical area and prone to fracture at the earliest. The failure predicted by the

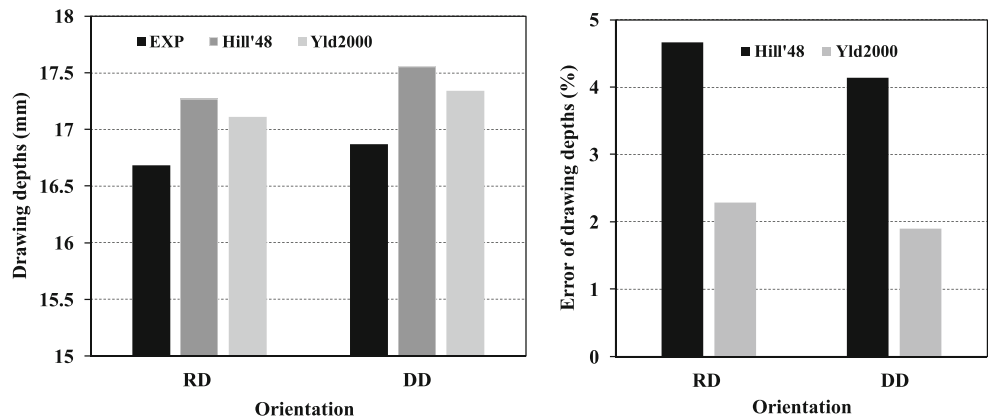
Fig. 23 Thickness changes of five different areas on the (a) RD and (b) samples during the cross die forming test of the examined aluminum sheet until experimental failure calculated by FE simulations coupled with the Yld2000-2d yield criterion



FFLC on the principal strain space in Fig. 22 was in accordance with that described by the FL in the space of equivalent

strain and stress triaxiality in Fig. 21. The other investigated zones on deformed sheet sample showed the strain paths,

Fig. 24 Comparisons of experimentally determined and predicted drawing depths of RD and DD samples at fracture for the investigated aluminum sheet grade AA5052-H32 in the cross die forming test



which developed in various regions of stress state. The variations of occurred stress states could be well correlated with those in the stress-strain space. The first, second and third areas underwent plastic deformations in the range between plane strain and biaxial tension. The fourth area was subjected to the stress regions between uniaxial and plane strain tension, whereas the fifth area experienced the stress states between in-plane shear and uniaxial tension. The RD samples also exhibited the strain paths of the individual areas of sheet similar to the DD samples. Small deviations of stress and strain developments on the RD and DD samples during the cross die forming test were due to the bending effect and anisotropic behavior of examined aluminum sheet.

Subsequently, through thickness fracture was studied by FE simulations coupled with the anisotropic Yld2000-2d yield criterion, in which thickness alterations of the same five areas during the cross die forming test were determined. The developments of changed thickness of sheet with increasing punch displacement were gathered for the RD and DD samples until experimental fracture emerged, as illustrated in Fig. 23(a) and (b), accordingly. The first area on both RD and DD samples showed a maximum thickness reduction of around 13% and constant thickness beyond the punch stroke of around 14 mm. The thickness of the second area was rapidly decreased from the displacement of 8 mm and attained a reduction of about 25%. The third area exhibited the smallest thickness decrease. The fourth area showed a continuous thickness decrease from the early forming state. For the fifth area, the RD sample showed a slight thickening, while the DD sample sustained a thinning. The similar thickness changes were also reported in Khalfallah et al. [57] and Carvalho-Resende et al. [63]. Generally, the thickness reductions of the DD sample were more significant than those of the RD sample.

Due to the material anisotropy fractures were observed at all corners close to the regions of punch radius in the case of DD sample, while the RD samples exhibited fractures at some corners, as seen in Figs. 15 and 17. The predicted strain distributions on both surfaces of the RD and DD samples during the cross die forming test were also noticeably different from the beginning until failure, as depicted in Fig. 16. Finally, the final drawing depths of formed RD and DD samples at the fracture state of cross die forming test were measured. The results from the experiments and corresponding FE simulations using the representative FFLCs generated by the Lou-Huh model coupled with different yield functions are compared in Fig. 24. It can be seen that the calculated achievable drawing depths of samples were considerably affected by the applied yield criteria. Obviously, the predictions of the FFLC based on the Yld2000-2d model were more accurate than those of the FFLC based on the Hill'48 model for the samples positioned in both directions with the largest error of around 2%. The non-quadratic Yld2000-2d yield criterion was more suitable for describing material under large plastic deformation and complex stress state than the Hill'48 yield function.

8 Conclusions

The plastic anisotropy effects on the forming limits of the aluminum sheet grade AA5052-H32 were investigated. The FLs of sheet were generated by using the Lou-Huh ductile fracture criterion coupled with the Hill'48 and Yld2000-2d yield function for different loading directions, namely, RD, DD and TD. The model constants were determined by the simple tensile tests of pure shear, uniaxial tension and plane strain samples. Subsequently, the FLs in the space of equivalent strain and stress triaxiality were transformed to FFLCs in the space of principal strains. To verify the applicability of the proposed FFLCs, the cross die forming test and square cup drawing test were conducted. The experimental results were then compared with those predicted by the corresponding FE simulations. The main findings of this work can be drawn as following.

- The constructed FLs incorporated a wide range of stress triaxiality values between about 0 and 0.677. Generally, the FLs predicted by the Lou-Huh model combined with the Yld2000-2d function were somewhat higher and could more precisely describe the experimental fracture points from the tensile and Marciniak tests of different samples at all stress states than those obtained by the Hill'48 function. Moreover, the unique anisotropic FL of the aluminum sheet was proposed, which represented the lowest plastic strain limits of all three sample orientations at all states of stress.
- The force-displacement curve, moment of failure onset and fracture sites of sheet samples positioned in the RD and DD in the cross die forming test and square cup drawing test were correctly predicted. The cross die shape sample exhibited a complex plastic deformation including all states of states of thin sheet. However, the fracture occurrences of cross die samples were mainly governed by the biaxial tension stress, while those of square cup samples were induced by the in-plane shear stress.
- Due to the material anisotropy fractures were observed at all edges close to the regions of punch radii of the DD sample, while the RD sample only exhibited fractures at some edges. The emerged cracks at the punch radii of sheets afterwards propagated in both circumferential directions. The fracture initiation was triggered first on the outer surface of cross die samples, whereas the crack onset occurred on the inner surface of square cup samples.
- The calculated achievable drawing depths of cross die shape samples were considerably affected by the applied yield criteria. Noticeably, the predictions of the FFLC based on the Lou-Huh model coupled with the Yld2000-2d function were more accurate than those coupled with the Hill'48 function for the samples

orientated in both directions with the largest error of around 2%.

Acknowledgements This research was funded by King Mongkut's University of Technology North Bangkok (contract no. KMUTNB-62-KNOW-15). The authors also wish to express their appreciation to KMUTNB for allowing the authors to access the FE software license ABAQUS2017. The authors are much obliged to the Department of Mechanical Engineering, KMUTT and Thai German Graduate School of Engineering (TGGS), KMUTNB for the ARAMIS system and AutoGrid, respectively. The authors acknowledge the Department of Production Engineering, Faculty of Engineering, KMUTNB for all other necessary research facilities. In addition, the authors are very grateful to Prof. Jeong Whan Yoon for providing the Yld2000–2d UMAT program.

Code availability Not applicable.

Funding This work was supported by King Mongkut's University of Technology North Bangkok (Grant number (KMUTNB-62-KNOW-15).

Data availability Not applicable.

Declarations

Competing interests The authors declare no competing interests.

References

- Sekhar KC, Narayanasamy R, Velmanirajan K (2014) Experimental investigations on microstructure and formability of cryorolled AA 5052 sheets. *Mater Des* 53:1064–1070. <https://doi.org/10.1016/j.matdes.2013.08.008>
- Keeler SP, Backofen WA (1963) Plastic instability and fracture in sheets stretched over rigid punches. *Trans ASM* 56:25–48
- Goodwin GM (1968) Application of strain analysis to sheet metal forming problems in the press shop. *Trans Soc Automotive* 25:1413–1424
- Bao YB, Wierzbicki T (2004) On fracture locus in the equivalent strain and stress triaxiality space. *Int J Mech Sci* 46:81–98
- Børvik T, Hopperstad OS, Pedersen KO (2010) Quasi-brittle fracture during structural impact of AA7075-T651 aluminum plates. *Int J Impact Eng* 37:537–551
- Khan AS, Liu H (2012) A new approach for ductile fracture prediction on Al 2024-T351 alloy. *Int J Plast* 35:1–12. <https://doi.org/10.1016/j.ijplas.2012.01.003>
- Khan AS, Liu H (2012) Strain rate and temperature dependent fracture criteria for isotropic and anisotropic metals. *Int J Plast* 37:1–15. <https://doi.org/10.1016/j.ijplas.2012.01.012>
- Lemaitre J (1985) A continuous damage mechanics model for ductile fracture. *J Eng Mater Technol* 107:83–89
- McClintock FA (1968) A criterion for ductile fracture by the growth of holes. *ASME J Appl Mech* 35:363–371
- Rice JR, Tracey DM (1969) On the ductile enlargement of voids in triaxial stress fields. *J Mech Phys Solids* 17:201–217
- Chu CC, Needleman A (1980) Void nucleation effects in biaxially stretched sheets. *J Eng Mater Technol* 102:249–256
- LeRoy G, Embury J, Edwards G, Ashby MF (1981) A model of ductile fracture based on the nucleation and growth of voids. *Acta Metall* 29:1509–1522
- Cockcroft MG, Latham DJ (1968) Ductility and the workability of metals. *J Inst Met* 96:33–39
- Brozzo P, DeLuca B, Rendina R (1972) A new method for the prediction of the formability limits of metal sheets. In: *Proceedings of the 7th Biennial Conference of IDDRG on Sheet Metal Forming and Formability*.
- Oh SI, Chen CC, Kobayashi S (1979) Ductile fracture in axisymmetric extrusion and drawing: part 2: workability in extrusion and drawing. *J Manuf Sci Eng* 101(1):36–44. <https://doi.org/10.1115/1.3439471>
- Oyane M, Sato T, Okimoto K, Shima S (1980) Criteria for ductile fracture and their applications. *J Mech Work Technol* 4:65–81. [https://doi.org/10.1016/0378-3804\(80\)90006-6](https://doi.org/10.1016/0378-3804(80)90006-6)
- Clift SE, Hartley P, Sturgess CEN, Rowe GW (1990) Fracture prediction in plastic deformation processes. *Int J Mech Sci* 32:1–17. [https://doi.org/10.1016/0020-7403\(90\)90148-C](https://doi.org/10.1016/0020-7403(90)90148-C)
- Ko YK, Lee JS, Huh H, Kim HK, Park SH (2007) Prediction of fracture in hub-hole expanding process using a new ductile fracture criterion. *J Mater Process Technol* 187:358–362. <https://doi.org/10.1016/j.jmatprotec.2006.11.071>
- Bai Y, Wierzbicki T (2010) Application of extended Mohr-Coulomb criterion to ductile fracture. *Int J Fract* 161:1–20. <https://doi.org/10.1007/s10704-009-9422-8>
- Lou YS, Huh H, Lim SJ, Pack KH (2012) New ductile fracture criterion for pre- diction of fracture forming limit diagrams of sheet metals. *Int J Solids Struct* 49:3605–3615. <https://doi.org/10.1016/j.ijsolstr.2012.02.016>
- Banabic D (2010) Sheet metal forming processes: Constitutive modelling and numerical simulation. Springer, Berlin Heidelberg
- Pack K, Roth CC (2016) The second Sandia Fracture Challenge: Blind prediction of dynamic shear localization and full fracture characterization. *Int J Fract* 198:197–220 <http://hdl.handle.net/1721.1/103311>
- Benzerger AA, Besson J, Pineau A (2004) Anisotropic ductile fracture. Part I: experiments. *Acta Mater* 52:4623–4638. <https://doi.org/10.1016/j.actamat.2004.06.020>
- Benzerger AA, Besson J, Pineau A (2004) Anisotropic ductile fracture. Part II: theory. *Acta Mater* 52:4639–4650. <https://doi.org/10.1016/j.actamat.2004.06.019>
- Beese AM, Luo M, Li Y, Bai Y, Wierzbicki T (2008) Partially coupled anisotropic fracture model for aluminum sheets. *Eng Fract Mech* 77:1128–1152. <https://doi.org/10.1016/j.engfracmech.2010.02.024>
- Luo M, Dunand M, Mohr D (2012) Experiments and modeling of anisotropic aluminum extrusions under multi-axial loading - Part II: Ductile fracture. *Int J Plast* 32-33:36–58. <https://doi.org/10.1016/j.ijplas.2011.11.001>
- Lou YS, Yoon JW (2015) Anisotropic behavior in plasticity and ductile fracture of an aluminum alloy. *Key Eng Mater* 651-653:163–168. <https://doi.org/10.4028/www.scientific.net/KEM.651-653.163>
- Park N, Huh H, Lim SJ, Lou YS, Kang YS, Seo MH (2017) Fracture-based forming limit criteria for anisotropic materials in sheet metal forming. *Int J Plast* 96:1–35. <https://doi.org/10.1016/j.ijplas.2016.04.014>
- Park N, Huh H, Yoon JW (2018) Anisotropic fracture forming limit diagram considering non-directionality of the equi-biaxial fracture strain. *Int J Solids Struct* 151:181–194. <https://doi.org/10.1016/j.ijsolstr.2018.01.009>
- Lou YS, Yoon JW (2018) Anisotropic yield function based on stress invariants for BCC and FCC metals and its extension to ductile fracture criterion. *Int J Plast* 101:125–155. <https://doi.org/10.1016/j.ijplas.2017.10.012>
- Li S, He J, Gu B, Zeng D, Xia ZC, Zhao Y, Lin ZQ (2018) Anisotropic fracture of advanced high strength steel sheets:

- experiment and theory. *Int J Plast* 103:95–118. <https://doi.org/10.1016/j.ijplas.2018.01.003>
32. Young WL (2005) Fracture prediction in metal sheets. PhD Thesis, MIT
 33. Bai Y (2008) Effect of loading history on necking and fracture. PhD Thesis, MIT
 34. Li Y, Luo M, Gerlach J, Wierzbicki T (2010) Prediction of shear-induced fracture in sheet metal forming. *J Mater Process Technol* 210:1858–1869. <https://doi.org/10.1016/j.jmatprotec.2010.06.021>
 35. Chen W, Song H, Lazarescu L, Xu Y, Zhang SH, Banabic D (2020) Formability analysis of hot-rolled dual-phase steel during the multistage stamping process of wheel disc. *Int J Adv Manuf Technol* 110:1563–1573. <https://doi.org/10.1007/s00170-020-05963-x>
 36. Manopulo N, Peters P, Hora P (2017) Assessment of anisotropic hardening models for conventional deep drawing processes. *Int J Mater Form* 10:623–631. <https://doi.org/10.1007/s12289-016-1306-7>
 37. Gorji M, Berisha B, Hora P, Barlat F (2016) Modeling of localization and fracture phenomena in strain and stress space for sheet metal forming. *Int J Mater Form* 9:573–584. <https://doi.org/10.1007/s12289-015-1242-y>
 38. Pack K, Tancogne-Dejean T, Gorji M, Mohr D (2018) Hosford-Coulomb ductile failure model for shell elements: Experimental identification and validation for DP980 steel and aluminum 6016-T4. *Int J Solids Struct* 51:214–232. <https://doi.org/10.1016/j.ijsolstr.2018.08.006>
 39. Talebi-Ghadikolaei H, Naein HM, Naeini HM, Mirzai MA, Alexandrov S, Gorji H (2019) Experimental and numerical investigation of failure during bending of AA6061 aluminum alloy sheet using the modified Mohr-Coulomb fracture criterion. *Int J Adv Manuf Technol* 105:5217–5237
 40. Panich S, Suranuntchai S, Jiratharnat S, Uthaisangsuk V (2016) A hybrid method for prediction of damage initiation and fracture and its application to forming limit analysis of advanced high strength steel sheet. *Eng Fract Mech* 166:97–127. <https://doi.org/10.1016/j.engfracmech.2016.08.025>
 41. Charoensuk K, Panich S, Uthaisangsuk V (2017) Damage initiation and fracture loci for advanced high strength steel sheets taking into account anisotropic behavior. *J Mater Process Technol* 248:218–235. <https://doi.org/10.1016/j.jmatprotec.2017.05.035>
 42. Dunand M, Mohr D (2010) Hybrid experimental-numerical analysis of basic ductile fracture experiments for sheet metals. *Int J Solids Struct* 47:1130–1142. <https://doi.org/10.1016/j.ijsolstr.2009.12.011>
 43. Butuc MC, Gracio JJ, Da Rocha AB (2006) An experimental and theoretical analysis on the application of stress-based forming limit criterion. *Int J Mech Sci* 48:414–429. <https://doi.org/10.1016/j.ijsolstr.2005.11.007>
 44. Stoughton TB (2000) A general forming limit criterion for sheet metal forming. *Int J Mech Sci* 42:1–17. [https://doi.org/10.1016/S0020-7403\(98\)00113-1](https://doi.org/10.1016/S0020-7403(98)00113-1)
 45. Barlat F, Brem JC, Yoon JW, Chung K, Dick RE, Lege DJ, Pourboghrat F, Choi SH, Chu E (2003) Plane stress yield function for aluminum alloy sheets—part 1: theory. *Int J Plast* 19:1297–1319. [https://doi.org/10.1016/S0749-6419\(02\)00019-0](https://doi.org/10.1016/S0749-6419(02)00019-0)
 46. Yoon JW, Barlat F, Dick RE, Chung K, Kang TJ (2004) Plane stress yield function for aluminum alloy sheets - part II: FE formulation and its implementation. *Int J Plast* 20:495–522. [https://doi.org/10.1016/S0749-6419\(03\)00099-8](https://doi.org/10.1016/S0749-6419(03)00099-8)
 47. Basak S, Panda SK (2019) Failure strains of anisotropic thin sheet metals: Experimental evaluation and theoretical prediction. *Int J Mech Sci* 151:356–374. <https://doi.org/10.1016/j.ijsolstr.2018.10.065>
 48. Panich S, Liewald M, Uthaisangsuk V (2018) Stress and strain based fracture forming limit curves for advanced high strength steel sheet. *Int J Mater Form* 11:643–661. <https://doi.org/10.1007/s12289-017-1378-z>
 49. Alharthi H, Hazra S, Alghamdi A, Banabic D, Dashwood R (2018) Determination of the yield loci of four sheet materials (AA6111-T4, AC600, DX54D+ Z, and H220BD+ Z) by using uniaxial tensile and hydraulic bulge tests. *Int J Adv Manuf Technol* 98:1307–1319. <https://doi.org/10.1007/s00170-018-2339-5>
 50. Prakash V, Kumar DR, Horn A, Hagenah H, Merklein M (2020) Modeling material behavior of AA5083 aluminum alloy sheet using biaxial tensile tests and its application in numerical simulation of deep drawing. *Int J Adv Manuf Technol* 106:1133–1148
 51. Nasser A, Yadav A, Pathak P, Altan T (2010) Determination of the flow stress of five AHSS sheet materials (DP 600, DP 780, DP 780-CR, DP 780-HY and TRIP 780) using the uniaxial tensile and the biaxial viscous pressure bulge (VPB) tests. *J Mater Process Technol* 210:429–436. <https://doi.org/10.1016/j.jmatprotec.2009.10.003>
 52. Bandstra JP, Koss DA (2004) A simulation of growth and coalescence of voids during ductile fracture. *Mater Sci Eng A* 387:399–403. <https://doi.org/10.1016/j.msea.2004.02.092>
 53. Kuwabara T, Hashimoto K, Iizukac E, Yoon JW (2013) Effect of anisotropic yield functions on the accuracy of hole expansion simulations. *J Mater Process Technol* 211:475–481. <https://doi.org/10.1016/j.jmatprotec.2010.10.025>
 54. Raghavan KS (1995) A simple technique to generate in-plane forming limit curves and selected applications. *Metall Trans A* 26:2075–2084. <https://doi.org/10.1007/BF02670679>
 55. Quak G (2008) Biaxial Testing of Sheet Metal: An experimental-numerical analysis. Eindhoven University of Technology, Eindhoven, Netherland, Master Thesis
 56. Beese AM, Luo N, Li Y, Bai Y, Wierzbicki T (2010) Partially coupled anisotropic fracture model for aluminum sheets. *Eng Fract Mech* 77:1128–1152. <https://doi.org/10.1016/j.engfracmech.2010.02.024>
 57. Khalfallah A, Alves JL, Oliveira MC, Menezes LF (2015) Influence of the characteristics of the experimental data set used to identify. *Simul Model Pract Theory* 53:15–44. <https://doi.org/10.1016/j.simpat.2015.02.007>
 58. Manopulo N, Hora P, Peters P, Gorji M (2015) An extended modified maximum force criterion for the prediction of localized necking under non-proportional loading. *Int J Plast* 75:189–203. <https://doi.org/10.1016/j.ijplas.2015.02.003>
 59. Gorji M, Berisha B, Manopulo N, Hora P (2016) Effect of through thickness strain distribution on shear fracture hazard and its mitigation by using multilayer aluminum sheets. *J Mater Process Technol* 232:19–33. <https://doi.org/10.1016/j.jmatprotec.2016.01.014>
 60. Gorji M, Mohr D (2018) Predicting shear fracture of aluminum 6016-T4 during deep drawing: Combining Yld-2000 plasticity with Hosford-Coulomb fracture model. *Int J Mech Sci* 137:105–120. <https://doi.org/10.1016/j.ijsolstr.2018.01.008>
 61. Habibi N, Ramazani A, Sundararaghavan V, Pahl U (2017) Failure predictions of DP600 steel sheets using various uncoupled fracture criteria. *Eng Fract Mech* 190:367–381. <https://doi.org/10.1016/j.engfracmech.2017.12.022>
 62. Jang I, Bae G, Song J, Kim H, Park N (2020) Fracture envelopes on the 3D-DIC and hybrid inverse methods considering loading history. *Mat Design* 194:108934. <https://doi.org/10.1016/j.matdes.2020.108934>
 63. Carvalho-Resende TC, Balan T, Bouvier S, Meraim FA, Sablin SS (2013) Numerical investigation and experimental validation of a plasticity model for sheet steel forming. *Model Simul Mater Sci Eng* 21(1):45006011. <https://doi.org/10.1088/0965-0393/21/1/015008>